



# ALMA Observations of Vibrationally Excited HC<sub>3</sub>N Lines Toward Orion KL

Yaping Peng<sup>1</sup>, Sheng-Li Qin<sup>1</sup>, Peter Schilke<sup>2</sup>, Álvaro Sánchez-Monge<sup>2</sup>, Yuefang Wu<sup>3</sup>, Tie Liu<sup>4</sup>, Di Li<sup>5</sup>, Thomas Möller<sup>2</sup>,  
Sheng-Yuan Liu<sup>6</sup>, Siyi Feng<sup>7</sup>, Ying Liu<sup>8</sup>, Gan Luo<sup>5</sup>, Li Zhang<sup>1</sup>, and Jia-Lei Rong<sup>1</sup>

<sup>1</sup> Department of Astronomy, Yunnan University, and Key Laboratory of Astroparticle Physics of Yunnan Province, Kunming, 650091, China; [pyp893@163.com](mailto:pyp893@163.com),  
[slqin@bao.ac.cn](mailto:slqin@bao.ac.cn), [lizhang@ynu.edu.cn](mailto:lizhang@ynu.edu.cn), [JiaLeiRong@163.com](mailto:JiaLeiRong@163.com)

<sup>2</sup> I. Physikalisches Institut, Universität zu Köln, Zùlpicher Str. 77, D-50937 Köln, Germany; [schilke@ph1.uni-koeln.de](mailto:schilke@ph1.uni-koeln.de),  
[sanchez@ph1.uni-koeln.de](mailto:sanchez@ph1.uni-koeln.de), [moeller@ph1.uni-koeln.de](mailto:moeller@ph1.uni-koeln.de)

<sup>3</sup> Department of Astronomy, Peking University, Beijing, 100871, China; [liutiepk@gmail.com](mailto:liutiepk@gmail.com)

<sup>4</sup> Korea Astronomy and Space Science Institute 776, Daedeokdaero, Yuseong-gu, Daejeon 305-348, Korea

<sup>5</sup> National Astronomical Observatories, Chinese Academy of Science, Chaoyang District, Datun Road 20A, Beijing, China; [ithaca.li@gmail.com](mailto:ithaca.li@gmail.com)

<sup>6</sup> Institute of Astronomy and Astrophysics, Academia Sinica, Taipei, Taiwan; [syliu@asiaa.sinica.edu.tw](mailto:syliu@asiaa.sinica.edu.tw)

<sup>7</sup> Max-Planck-Institut für Extraterrestrische Physik, Giessenbachstrasse 1, D-85748, Garching, Germany; [syfeng@mpe.mpg.de](mailto:syfeng@mpe.mpg.de)

<sup>8</sup> Department of Physics and Hebei Advanced Thin Film Laboratory, Hebei Normal University, Shijiazhuang 050024, China; [yliu@mail.hebtu.edu.cn](mailto:yliu@mail.hebtu.edu.cn)

Received 2016 October 17; revised 2017 January 5; accepted 2017 January 19; published 2017 March 1

## Abstract

We present high spatial resolution ALMA observations of vibrational transitions of HC<sub>3</sub>N toward Orion KL in the 214–247 GHz frequency band. 41 transitions of HC<sub>3</sub>N in 7 vibrationally excited states, and 23 transitions of <sup>13</sup>C isotopologues of HC<sub>3</sub>N in 2 vibrational states are detected. The line images show that vibrationally excited HC<sub>3</sub>N lines originate mainly from the hot core of Orion and IRc7. The images of HC<sub>3</sub>N vibrationally excited lines show that the line emission peaks associated with the hot core move from south to northeast as  $E_u$  increases. Based on multiple transitions of each vibrationally excited state, we performed local thermodynamic equilibrium calculations in the XCLASS suite toward the hot core and IRc7 positions. Generally, transitions in highly excited states have higher rotational temperatures and lower column densities. The rotational temperatures and column densities of the hot core range from 93 to 321 K, and from  $1.0 \times 10^{14}$  to  $4.9 \times 10^{16} \text{ cm}^{-2}$ , respectively. Lower rotational temperatures ranging from 88 to 186 K and column densities from  $1.0 \times 10^{14}$  to  $3.2 \times 10^{16} \text{ cm}^{-2}$  are obtained toward IRc7. The facts that the hot core emission peaks of vibrationally excited HC<sub>3</sub>N lines move from south to northeast with increasing  $E_u$ , and that higher-energy HC<sub>3</sub>N lines have higher rotational temperatures and lower column densities, appear to support that the hot core is externally heated. The emission peaks are moving along the major axis of the SiO outflow, which may indicate that higher-energy HC<sub>3</sub>N transitions are excited by interaction between pre-existing dense medium and shocks generated by SiO outflows.

**Key words:** ISM: abundances – ISM: individual objects (Orion KL) – ISM: molecules – radio lines: ISM – stars: formation

**Supporting material:** figure set

## 1. Introduction

The Orion Kleinmann-Low (hereafter, Orion KL) nebula is the closest ( $414 \pm 7$  pc) site of massive star formation (Menten et al. 2007). It is an atypical region in the Orion Molecular Cloud 1 (hereafter, OMC-1; Wynn-Williams et al. 1984), containing a number of luminous embedded infrared sources. The known infrared sources are discussed in Shuping et al. (2004). Among them, IRc2 and IRc7 are very compact infrared sources (Gezari et al. 1992), with IRc7 thought to contain an embedded young stellar object (YSO; Simpson et al. 2006). IRc2 is not self-luminous, but is illuminated and heated by the embedded luminous YSO located at Source I (Okumura et al. 2011). In the region, a radio continuum source named Radio Source I is coincident with the centroid of a group of SiO masers first reported by Menten & Reid (1995), and is likely the driving source of a thermal SiO outflow (Zapata et al. 2012). Observations of continuum and molecular lines at millimeter and submillimeter wavelengths have spatially resolved Orion KL into several components (e.g., Blake et al. 1987), namely: hot core, compact ridge, extended ridge, and plateau. Different physics, kinematics, and chemistry have been revealed

(Tercero et al. 2010; Neill et al. 2013; Crockett et al. 2014). The hot core is a hot ( $T_{\text{kin}} \geq 150$  K) and dense ( $\geq 10^7 \text{ cm}^{-3}$ ) gas clump located  $\sim 1''$  southeast of Source I, with a velocity  $v_{\text{LSR}}$  of 4–6 km s<sup>-1</sup> and line width  $\Delta v$  of 7–12 km s<sup>-1</sup> (e.g., Schilke et al. 1997; Wilson et al. 2000; Crockett et al. 2014). It has a non-uniform temperature distribution (Crockett et al. 2014). The Compact Ridge is another important component in Orion KL, with a lower density ( $\sim 10^6 \text{ cm}^{-3}$ ) and temperature ( $\sim 80$ –280 K) compared to the hot core (e.g., Beuther et al. 2005; Persson et al. 2007; Wang et al. 2010; Favre et al. 2011). Orion KL is also one of the most molecular line-rich star-forming regions (Blake et al. 1987, 1996; Schilke et al. 1997, 2001; Persson et al. 2007; Tercero et al. 2010). Previous single-dish and interferometric observations suggested that nitrogen-bearing complex molecules (e.g., CH<sub>3</sub>CN, C<sub>2</sub>H<sub>3</sub>CN and C<sub>2</sub>H<sub>5</sub>CN) are more abundant in the hot core, whereas oxygen-bearing molecules mainly dominate the chemistry of the compact ridge (e.g., Blake et al. 1987; Wright et al. 1996; Liu et al. 2002; Beuther et al. 2005). Recently, higher spatial resolution observations showed that nitrogen-bearing species (e.g., C<sub>2</sub>H<sub>5</sub>CN, C<sub>2</sub>H<sub>3</sub>CN, and CH<sub>3</sub>CN) have their emission extended toward IRc7, and are not only associated with the hot core (e.g.,

Blake et al. 1996; Friedel & Snyder 2008; Wang et al. 2010; Widicus Weaver & Friedel 2012; Feng et al. 2015). Note that another gas component located north of the hot core (hereafter, HC-north) was also detected by  $C_2H_5CN$ ,  $C_2H_3CN$ , and  $CH_3CN$  transitions.

Chemical models suggest that rich molecular lines may originate from grain-surface reactions as hot cores warm up (Garrod et al. 2008). Orion’s hot core is a molecular line-rich object, but the heating source is not clear yet. In this sense, cyanoacetylene ( $HC_3N$ ) is a very suitable molecule to probe the physical conditions and kinematics in hot cores, because it has widely been detected in high-mass star-forming regions (e.g., Belloche et al. 2013; Sánchez-Monge et al. 2013, 2014) and can be excited, not only in the ground state, but also in several vibrationally excited states (Thorwirth et al. 2000). In Orion KL, a few transitions of the vibrationally excited  $HC_3N$  in  $v_7 = 1$ ,  $v_7 = 2$  and  $v_6 = 1$  were detected with single-dish telescopes (e.g., Clark et al. 1976; Goldsmith et al. 1982, 1983, 1985). However, the low spatial resolution observations can not provide accurate information on the spatial distribution of  $HC_3N$   $v_7 = 1$ ,  $v_7 = 2$  and  $v_6 = 1$ . Currently available interferometric observations showed that the emission peak of  $HC_3N$   $v_7 = 1$  is near the hot core continuum peak (Blake et al. 1996; de Vicente et al. 2002; Feng et al. 2015). However, in order to investigate the physical conditions and heating mechanism in Orion KL, a larger number of highly excited  $HC_3N$  lines are required.

In this paper, we present a multi-transition study of vibrationally excited  $HC_3N$  states observed with ALMA in band 6, achieving a higher spatial resolution, better sensitivity, and improved image fidelity compared to previous studies. The paper is organized as follows. In Section 2, we present the observations. The results and data analyses are presented in Section 3. A general discussion is in Section 4. We summarize the results in Section 5.

## 2. Observations

### 2.1. ALMA observations

We used data from the ALMA science verification (SV) program.<sup>9</sup> The observations were carried with  $16 \times 12$  m antennas in 2012 January. The phase center of the observations is R.A.(J2000) =  $05^h35^m14^s.35$  and decl.(J2000) =  $-05^\circ22'35''.00$ . The baseline lengths range from 17 to 265 m. A total of 20 spectral windows covering the frequency range from 214 to 247 GHz were used. Each spectral window has a frequency width of 1.875 GHz, and consists of 3840 channels with a uniform spectral resolution of 0.448 MHz ( $\sim 0.7$  km s<sup>-1</sup>). The primary beam size of each 12 m antenna is about 30". Callisto and the quasar J0607-085 were used for the flux and phase calibration, respectively.

The calibrated UV data were exported to Miriad format, and images were made using the Miriad software package (Sault et al. 1995). The CLEAN algorithm with natural weighting was used for deconvolution. The continuum map was constructed from line-free channels extracted in the spectral window 14, as shown in Figure 1. The synthesized beam size and the rms noise level for the continuum are  $1''.92 \times 1''.41$  (P.A. =  $-14^\circ.4$ ) and  $0.01$  Jy beam<sup>-1</sup>, respectively. The 1 Jy beam<sup>-1</sup> corresponds to a main beam brightness temperature of  $\sim 9$  K. A two-dimensional

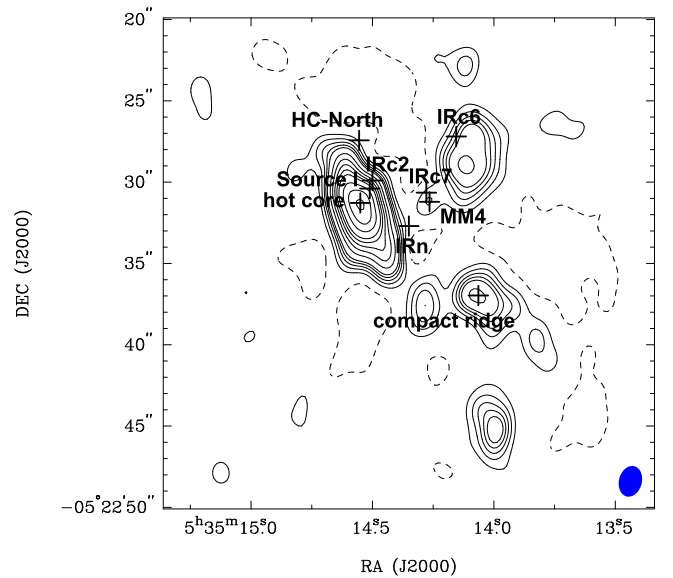


**Figure 1.** Continuum image at 224 GHz. The synthesized beam is shown in the bottom right corner. The contour levels are  $(-4, 4, 8, 12, 16, 20, 30, 40, 50, 60, 70, 90, 110, 130) \times 0.01$  Jy beam<sup>-1</sup>. The positions of hot core, HC-North, compact ridge, MM4, Source I, IRn, IRc2, IRc6, and IRc7 are denoted with cross symbols.

Gaussian fitting was made to the continuum image. The peak intensity and total integrated flux of the continuum emission are  $1.31 \pm 0.10$  Jy beam<sup>-1</sup> and  $5.08 \pm 0.37$  Jy, respectively. The synthesized beam size with natural weighting and rms noise level of the spectral images are approximately  $1''.82 \times 1''.44$  (P.A. =  $-4^\circ.6$ ) and  $0.03$  Jy beam<sup>-1</sup> per channel. In Figure 1, we indicate the position of different objects, namely: the hot core, the hot core north component (hereafter HC-North), the compact ridge, and the millimeter continuum source MM4 (Wu et al. 2014), along with the known infrared sources IRn, IRc2, IRc6, and IRc7 (Shuping et al. 2004), and radio Source I (Churchwell et al. 1987).

### 2.2. Single-dish Observations with the IRAM 30 m Telescope

IRAM 30 m single-dish observations of the Orion KL region were carried out on 2012 November 30 (PI: S. Feng, Feng et al. 2015). The observations cover frequencies 213.370–221.150 GHz (lower sideband) and 229.051–236.831 GHz (upper sideband), with velocity resolution of  $\sim 0.255$  km s<sup>-1</sup>. The beam size is  $\sim 11''.3$  in the upper sideband and  $\sim 11''.8$  in the lower sideband. The forward efficiency and main beam efficiency are 92% and 58%, respectively. The observations and data reduction are described in detail by Feng et al. (2015).

Single-dish observations trace the large-scale structure, whereas interferometric observations will filter out diffuse gas component and concentrate on compact part of the cloud. The IRAM 30 m single-dish observations were used to complement the short spacing information of ALMA  $HC_3N$  observations. The IRAM 30 m single-dish data were first converted to Miriad format, and then combined with the ALMA data using the task MOSMEM. To compare with ALMA data, we convolve images to have same beam size as that of the ALMA data.

<sup>9</sup> The data are available to the public and can be accessed from the ALMA-SV website at <https://almascience.nrao.edu/alma-data/science-verification>.

### 3. Results And Analysis

#### 3.1. Line Identification and LTE Calculation

We identify spectral line transitions and model the data using the eXtended CASA Line Analysis Software Suite (XCLASS; Möller et al. 2015), which accesses the Cologne Database for Molecular Spectroscopy (CDMS; Müller et al. 2001, 2005; <http://cdms.de>) and Jet Propulsion Laboratory (JPL; Pickett et al. 1998; <http://spec.jpl.nasa.gov>) molecular databases. Under the assumption of local thermodynamical equilibrium (LTE), XCLASS takes the beam dilution, the line opacity, and line blending into account (Möller et al. 2015), the expected intensities are related to the upper-level energies and the line strength  $S\mu^2$  of the transitions. The main modeling parameters of XCLASS for each molecule are the source size, the rotational temperature, the column density, the line full width at half maximum, and the velocity offset with respect to the systemic velocity of the object. The source sizes are obtained by two-dimension Gaussian fits to the line images. The velocity offsets and line widths are derived from Gaussian fits to the spectra. The above parameters are used as initial guesses, and then MAGIX (Modeling and Analysis Generic Interface for eXternal numerical codes; Möller et al. 2013) is used to optimize the fit and find the best solution. Different optimization algorithms can be used within MAGIX to explore the parameter space and minimize the  $\chi^2$  distribution space (Möller et al. 2013). Therefore, the combined usage of XCLASS and MAGIX provides the best fit to the data.

To identify lines, we set the following constraints (Snyder et al. 2005; Brouillet et al. 2015): the rest frequency must be reliable; all detected transitions for a given species must have similar LSR velocity of the source; the transitions at different frequency have different beam dilution effects; for a specific species, transitions having similar excitation condition should have similar spatial distributions and intensities. We have identified about 77 lines of HC<sub>3</sub>N and its <sup>13</sup>C isotopologues in ground and vibrationally excited states over the full ALMA band 6. In this work, all lines below the 3 $\sigma$  level are ignored. Moreover, we excluded those HC<sub>3</sub>N transitions that are clearly affected by blending with other molecules, along with weak HC<sub>3</sub>N transitions that are too faint to have been detected unambiguously. HC<sub>3</sub>N and its <sup>13</sup>C isotopologues in each excited state are fitted independently. In Figure 2, we show the model spectra (red curve) overlaid on the observed spectra using ALMA data alone (black curve) and using combined data (green dashed curve: ALMA+IRAM), toward the hot core, HC-North and IRc7 positions. One can see that each of unblended lines of <sup>13</sup>C and <sup>15</sup>N isotopologues of HC<sub>3</sub>N and each of HC<sub>3</sub>N lines in vibrational states, has almost same spectral profile and peak intensity in the two data sets (ALMA and ALMA+IRAM). Although two transitions of HC<sub>3</sub>N  $\nu = 0$  are observed with both ALMA and IRAM, the peak intensities of the combined data are much higher than those of the ALMA data alone (see Figure 2). Thus, one can safely use higher-energy transitions and isotopologues of HC<sub>3</sub>N from the ALMA data alone for data modeling. The derived parameters from three positions, including line width  $\Delta v$ , rotational temperature  $T_{\text{rot}}$ , and total column density  $N_{\text{T}}$  are listed in Table 1. In each state, all transitions have similar optical depths ( $\tau$ ), we list the mean optical depth in Table 1.

#### 3.1.1. HC<sub>3</sub>N and Its <sup>13</sup>C Isotopologues in the Ground State

Four transitions of HC<sub>3</sub>N  $\nu = 0$  are detected toward the three positions (hot core, HC-North, and IRc7) in our observations. All of them showed complicated line profiles that may be caused by large optical depths or complex kinematics. The <sup>13</sup>C and <sup>15</sup>N isotopologues of HC<sub>3</sub>N in the ground state are detected toward the three positions. Twelve, thirteen, and twelve transitions of <sup>13</sup>C isotopologues, including HC<sup>13</sup>CCN, HCC<sup>13</sup>CN, and H<sup>13</sup>CCCN are detected toward the hot core, HC-North, and IRc7, respectively. Three transitions of HCCC<sup>15</sup>N are detected toward the three positions. Table 3 summarizes the observations of <sup>13</sup>C and <sup>15</sup>N isotopologues of HC<sub>3</sub>N  $\nu = 0$ . The line parameters in this table are derived from Gaussian fits to the lines. From left to right in Table 3, the parameters are the molecular name, rest frequency, quantum numbers, the line strength  $S\mu^2$ , and the upper level energies  $E_u$  of each line. The LSR velocity, full width at half-maximum, and peak intensity from each position derived from the Gaussian fits are listed in columns 6 to 14. The last column lists the 1 $\sigma$  channel rms noise level of each line.

HC<sup>13</sup>CCN  $\nu = 0$  with  $E_u$  in the range 130–165 K are well-fitted with a rotational temperature of  $93 \pm 10$  K and a column density of  $(6.0 \pm 2.0) \times 10^{14} \text{ cm}^{-2}$  for the hot core,  $90 \pm 11$  K and  $(5.0 \pm 2.0) \times 10^{14} \text{ cm}^{-2}$  for HC-North, and  $88 \pm 19$  K and  $(2.0 \pm 1.0) \times 10^{14} \text{ cm}^{-2}$  for IRc7. We used these temperatures to model HCC<sup>13</sup>CN, H<sup>13</sup>CCCN, and HCCC<sup>15</sup>N. The resulting column densities of three <sup>13</sup>C isotopologues of HC<sub>3</sub>N are all  $6 \times 10^{14} \text{ cm}^{-2}$ ,  $5 \times 10^{14} \text{ cm}^{-2}$  and  $2 \times 10^{14} \text{ cm}^{-2}$  toward the hot core, HC-North, and IRc7, respectively (see Table 1). The column density of the <sup>15</sup>N isotopologue is  $\sim 1 \times 10^{14} \text{ cm}^{-2}$  at the three positions (see Table 1).

#### 3.1.2. HC<sub>3</sub>N and Its <sup>13</sup>C Isotopologues in Vibrationally Excited States

The transitions of HC<sub>3</sub>N in the bending vibrationally excited states ( $\nu_7 = 1$ ,  $\nu_7 = 2$ ,  $\nu_7 = 3$ ,  $\nu_6 = 1$ , and  $\nu_5 = 1$ ) spanning a broad range of upper-level energies (452–1111 K) are detected toward the three positions. The stretching vibrational states ( $\nu_4 = 1$ ,  $\nu_4 = \nu_7 = 1$ ) of HC<sub>3</sub>N with upper-level energies in the range of 1376–1749 K are also detected, but are rather weaker compared to the bending, vibrationally excited states. Some <sup>13</sup>C isotopologues of HC<sub>3</sub>N, including H<sup>13</sup>CCCN, HC<sup>13</sup>CCN, and HCC<sup>13</sup>CN in their  $\nu_7 = 1$  and  $\nu_7 = 2$  vibrationally excited states are detected. Most of these weak transitions are blended with other lines. Table 4 summarizes the parameters of vibrationally excited HC<sub>3</sub>N transitions. The fitted rotational temperature and column density of each vibrational state are discussed below.

HC<sub>3</sub>N  $\nu_7 = 1$ : Eight transitions of  $\nu_7 = 1$  with  $E_u$  of 452–486 K are detected at each position. The best fit parameters are  $T_{\text{rot}} = 184 \pm 13$  K and  $N_{\text{T}} = (3.8 \pm 1.9) \times 10^{16} \text{ cm}^{-2}$  toward the hot core,  $168 \pm 7$  K and  $(2.0 \pm 0.7) \times 10^{16} \text{ cm}^{-2}$  toward HC-North, and  $148 \pm 15$  K and  $(2.5 \pm 0.7) \times 10^{16} \text{ cm}^{-2}$  toward IRc7. In this state, there are 8, 14, and 5 unblended lines of <sup>13</sup>C isotopologues in the hot core, HC-North, and IRc7, respectively. The temperatures of <sup>13</sup>C isotopologues in this state are assumed to be the same as those of the main species. Toward the hot core, the column densities of H<sup>13</sup>CCCN and HCC<sup>13</sup>CN are estimated to be  $(7 \pm 2) \times 10^{14}$  and  $(7 \pm 1) \times 10^{14} \text{ cm}^{-2}$ , respectively. Toward HC-North, the column densities of H<sup>13</sup>CCCN,

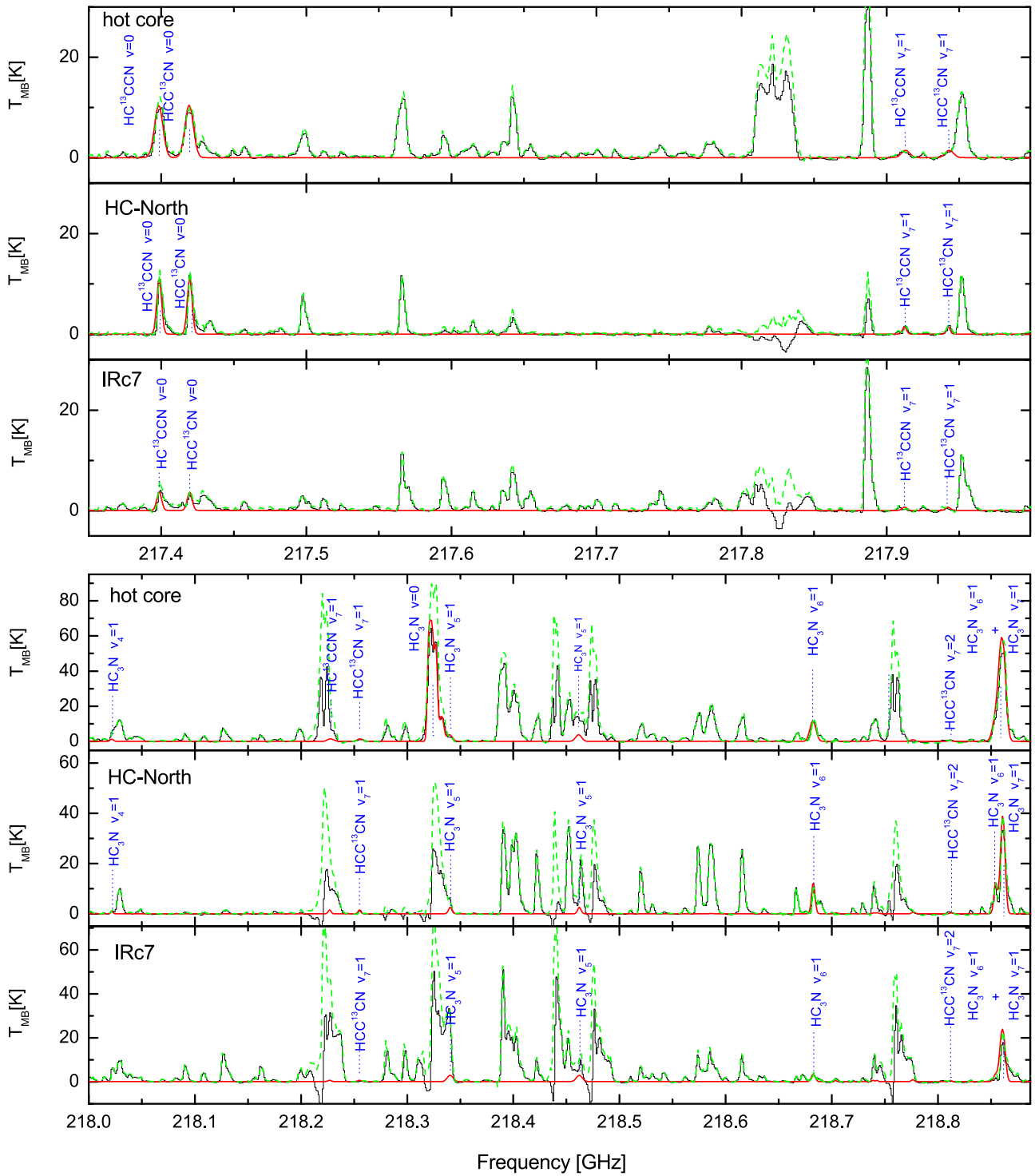


**Figure 2.** Sample spectra of  $\text{HC}_3\text{N}$  and its  $^{13}\text{C}$  isotopologues in ground state and vibrational states detected in the Orion KL from 217 to 219 GHz. Each panel consists of three plots: the top, middle, and bottom plots show the spectra from the hot core, HC-North, and IRc7, respectively. The frequency scale is in terms of rest frequency. The black curve is the observed spectra, and red curve indicates the simulated spectra. The green dashed curve indicates the observed spectra from the combined ALMA and IRAM 30 m data.

(The complete figure set (20 images) is available.)

$\text{HC}^{13}\text{CCN}$ , and  $\text{HCC}^{13}\text{CN}$  are about  $(4 \pm 1) \times 10^{14} \text{ cm}^{-2}$ . Toward IRc7, the column density of  $\text{HCC}^{13}\text{CN}$  is  $(5 \pm 1) \times 10^{14} \text{ cm}^{-2}$ .

$\text{HC}_3\text{N } v_7 = 2$ : Apart from  $v_7 = 2$  in the  $J = 24-23$ ,  $l = 2f$  state, which is blended with  $\text{HNCO } v = 0$ , eight isolated lines with  $E_u$  ranging from 773 to 799 K are identified toward each

position. The LTE fitting gives  $T_{\text{rot}} = 198 \pm 8 \text{ K}$  and  $N_{\text{T}} = (4.9 \pm 2.8) \times 10^{16} \text{ cm}^{-2}$  for the hot core,  $180 \pm 11 \text{ K}$  and  $(3.9 \pm 1.8) \times 10^{16} \text{ cm}^{-2}$  for HC-North, and  $157 \pm 16 \text{ K}$  and  $(3.2 \pm 1.8) \times 10^{16} \text{ cm}^{-2}$  for IRc7. In this state, there are eight, nine, and six unblended lines of  $^{13}\text{C}$  isotopologues in the hot core, HC-North, and IRc7, respectively. We use the same

**Table 1**  
Model Fitting Results of HC<sub>3</sub>N in Ground and Vibrational States

State	Hot Core				HC-North				IRc7			
	$\Delta v$ (km s <sup>-1</sup> )	$T_{\text{rot}}$ (K)	$N_{\text{T}}$ (10 <sup>16</sup> cm <sup>-2</sup> )	$\tau$	$\Delta v$ (km s <sup>-1</sup> )	$T_{\text{rot}}$ (K)	$N_{\text{T}}$ (10 <sup>16</sup> cm <sup>-2</sup> )	$\tau$	$\Delta v$ (km s <sup>-1</sup> )	$T_{\text{rot}}$ (K)	$N_{\text{T}}$ (10 <sup>16</sup> cm <sup>-2</sup> )	$\tau$
HC <sub>3</sub> N $v_7 = 1$	9.3	184 ± 13	3.8 ± 1.6	0.5	6.3	168 ± 7	2.0 ± 0.7	0.2	7.5	148 ± 15	2.5 ± 0.7	0.5
HC <sub>3</sub> N $v_7 = 2$	9.1	198 ± 8	4.9 ± 2.3	0.2	6.1	180 ± 11	3.9 ± 1.8	0.3	7.0	157 ± 16	3.2 ± 1.8	0.09
HC <sub>3</sub> N $v_7 = 3$	8.0	237 ± 10	2.9 ± 0.7	0.03	5.0	214 ± 12	2.1 ± 1.2	0.03	4.0	186 ± 14	0.7 ± 0.4	0.009
HC <sub>3</sub> N $v_6 = 1$	9.0	209 ± 14	3.9 ± 2.2	0.1	5.0	199 ± 19	3.6 ± 1.9	0.017	6.0	176 ± 9	1.4 ± 0.8	0.06
HC <sub>3</sub> N $v_5 = 1$	8.0	237 ± 12	2.9 ± 0.8	0.03	5.0	214 ± 16	2.1 ± 0.9	0.03	...	...	...	...
HC <sub>3</sub> N $v_4 = 1$	5.2	321 ± 78	0.9 ± 0.5	0.007	3.2	300 ± 108	0.6 ± 0.3	0.003	...	...	...	...
H <sup>13</sup> CCCN $v = 0$	9.0	93 ± 10	0.06 ± 0.02	0.17	5.0	90 ± 11	0.05 ± 0.01	0.2	5.2	88 ± 19	0.020 ± 0.008	0.08
HC <sup>13</sup> CCN $v = 0$	9.0	93 ± 10	0.06 ± 0.01	0.17	5.0	90 ± 11	0.05 ± 0.01	0.2	5.2	88 ± 19	0.020 ± 0.006	0.08
HCC <sup>13</sup> CN $v = 0$	9.0	93 ± 10	0.06 ± 0.01	0.17	5.0	90 ± 11	0.05 ± 0.01	0.2	5.2	88 ± 19	0.020 ± 0.006	0.08
HCCC <sup>15</sup> N $v = 0$	6.2	93 ± 10	0.010 ± 0.004	0.5	4.0	90 ± 11	0.010 ± 0.003	0.2	5.1	88 ± 19	0.010 ± 0.003	0.5
H <sup>13</sup> CCCN $v_7 = 1$	9.0	184 ± 13	0.07 ± 0.02	0.01	4.0	168 ± 7	0.04 ± 0.01	0.03	...	...	...	...
HC <sup>13</sup> CCN $v_7 = 1$	...	...	...	...	4.0	168 ± 7	0.04 ± 0.01	0.03	...	...	...	...
HCC <sup>13</sup> CN $v_7 = 1$	9.0	184 ± 13	0.07 ± 0.01	0.01	4.0	168 ± 7	0.040 ± 0.006	0.03	4.5	148 ± 15	0.05 ± 0.01	0.01
H <sup>13</sup> CCCN $v_7 = 2$	6.0	198 ± 8	0.09 ± 0.03	0.004	4.0	180 ± 11	0.07 ± 0.01	0.003	...	...	...	...
HC <sup>13</sup> CCN $v_7 = 2$	6.0	198 ± 8	0.09 ± 0.01	0.004	4.0	180 ± 11	0.07 ± 0.01	0.003	3.0	157 ± 16	0.07 ± 0.01	0.007
HCC <sup>13</sup> CN $v_7 = 2$	6.0	198 ± 8	0.09 ± 0.01	0.004	4.0	180 ± 11	0.07 ± 0.01	0.003	...	...	...	...

**Table 2**  
<sup>13</sup>C Isotopologue Ratios

Ratio	Hot Core	HC-North	IRc7
HC <sub>3</sub> N $\nu_7 = 1$ /H <sup>13</sup> CCCN $\nu_7 = 1$			
HC <sub>3</sub> N $\nu_7 = 1$ /HC <sup>13</sup> CCN $\nu_7 = 1$	54 ± 25	50 ± 20	50 ± 17
HC <sub>3</sub> N $\nu_7 = 1$ /HCC <sup>13</sup> CN $\nu_7 = 1$			
HC <sub>3</sub> N $\nu_7 = 2$ /H <sup>13</sup> CCCN $\nu_7 = 2$			
HC <sub>3</sub> N $\nu_7 = 2$ /HC <sup>13</sup> CCN $\nu_7 = 2$	54 ± 28	56 ± 27	46 ± 26
HC <sub>3</sub> N $\nu_7 = 2$ /HCC <sup>13</sup> CN $\nu_7 = 2$			

rotational temperature as those of the main species for the isotopologues to measure column densities of about  $(9 \pm 1) \times 10^{14} \text{ cm}^{-2}$ . Toward HC-North, the column densities are  $(7 \pm 1) \times 10^{14} \text{ cm}^{-2}$ . Toward IRc7, the column density of HC<sup>13</sup>CCN is estimated to be  $(7 \pm 1) \times 10^{14} \text{ cm}^{-2}$ .

HC<sub>3</sub>N  $\nu_7 = 3$ : Five unblended HC<sub>3</sub>N  $\nu_7 = 3$  lines are detected toward the hot core and HC-North. The derived parameters are  $T_{\text{rot}} = 237 \pm 10 \text{ K}$ ,  $N_{\text{T}} = (2.9 \pm 0.7) \times 10^{16} \text{ cm}^{-2}$  for the hot core, and  $214 \pm 12 \text{ K}$ ,  $(2.1 \pm 1.2) \times 10^{16} \text{ cm}^{-2}$  for HC-North. We note that the column density for HC-North is not much lower than that of the hot core. As for IRc7,  $T_{\text{rot}} = 186 \pm 14 \text{ K}$  and  $N_{\text{T}} = (7 \pm 4) \times 10^{15} \text{ cm}^{-2}$  are obtained from the best fit to three unblended lines.

HC<sub>3</sub>N  $\nu_6 = 1$ : Eight HC<sub>3</sub>N  $\nu_6 = 1$  transitions with upper level energies of 848–883 K are detected. We derive  $209 \pm 14 \text{ K}$  and  $(3.9 \pm 3.7) \times 10^{16} \text{ cm}^{-2}$  toward the hot core. Similar values ( $199 \pm 19 \text{ K}$  and  $(3.6 \pm 1.9) \times 10^{16} \text{ cm}^{-2}$ ) are derived toward HC-North. The rotational temperature and column density are  $176 \pm 9 \text{ K}$  and  $(1.4 \pm 0.8) \times 10^{16} \text{ cm}^{-2}$  for IRc7.

HC<sub>3</sub>N  $\nu_5 = 1$ : Using six unblended lines,  $T_{\text{rot}} = 237 \pm 12 \text{ K}$  and  $N_{\text{T}} = (2.9 \pm 0.8) \times 10^{16} \text{ cm}^{-2}$  is measured for the hot core, and  $214 \pm 16 \text{ K}$  and  $(2.1 \pm 0.9) \times 10^{16} \text{ cm}^{-2}$  for HC-North. All the HC<sub>3</sub>N  $\nu_5 = 1$  transitions are heavily blended with other lines at the IRc7 position, which prevents us from determining the physical parameters.

HC<sub>3</sub>N  $\nu_4 = 1$ : Three HC<sub>3</sub>N  $\nu_4 = 1$  unblended lines with  $E_{\text{u}}$  of 1376–1410 K are observed toward the hot core and HC-North. The intensities of the  $\nu_4 = 1$  transitions at the IRc7 position are below the detection limit. We derived  $321 \pm 78 \text{ K}$  and  $(9 \pm 5) \times 10^{15} \text{ cm}^{-2}$  for the hot core, and  $300 \pm 108 \text{ K}$  and  $(6 \pm 3) \times 10^{15} \text{ cm}^{-2}$  for the HC-North position.

HC<sub>3</sub>N  $\nu_4 = \nu_7 = 1$ : Four transitions of  $\nu_4 = \nu_7 = 1$  in  $J = 25\text{--}24$ ,  $l = 1e$ ,  $J = 26\text{--}25$ ,  $l = 1e$ ,  $J = 26\text{--}25$ ,  $l = 1f$  and  $J = 27\text{--}26$ ,  $l = 1e$  are detected only toward the hot core. However, these transitions are weak and partially blended with other features, which prevents us from deriving accurate rotational temperatures and column densities.

### 3.1.3. Carbon Isotopic Ratio

HC<sub>3</sub>N and its <sup>13</sup>C isotopologues in vibrationally excited states ( $\nu_7 = 1$  and  $\nu_7 = 2$ ) are optically thin (see optical depths in Columns 5, 9, and 13 of Table 1). Therefore, we can obtain reliable measurements of the <sup>12</sup>C/<sup>13</sup>C ratio. We derive this ratio from the column densities of HC<sub>3</sub>N and its <sup>13</sup>C isotopologues in the selected vibrational levels, and list them in Table 2. No obvious differences for the isotopic ratio are found among the different vibrational states. An average value of <sup>12</sup>C/<sup>13</sup>C =  $52 \pm 24$  is obtained. For a distance of 414 pc to the Sun, and considering the <sup>12</sup>C/<sup>13</sup>C ratio as function of Galactic center distance of <sup>12</sup>C/<sup>13</sup>C =  $(7.80 \pm 1.37)D_{\text{GC}}$

$\text{kpc}^{-1} + (-3.53 \pm 10.63)$  (Langer & Penzias 1990, 1993), a value of  $56 \pm 11$  is obtained. This equation gives a lower limit to the actual ratio. Our result of <sup>12</sup>C/<sup>13</sup>C =  $52 \pm 24$  is in agreement with the value derived from the equation, and is also consistent with previous estimations of  $43 \pm 7$  (Savage et al. 2002),  $45 \pm 20$  (Tercero et al. 2010),  $57 \pm 14$  (Persson et al. 2007) and  $63 \pm 17$  (Gong et al. 2015).

### 3.2. Spatial Distribution

The velocity integrated intensity map of H<sup>13</sup>CCCN  $\nu = 0$  observed with ALMA (black contours) is shown in Figure 3, in which the combined ALMA+IRAM data (red contours) are overlaid. The positions of sources I, IRc7, and IRc6 are marked with solid circles, whereas the cross symbols denote the continuum peak positions of the hot core, compact ridge, and MM4. The ALMA observations show that, unlike the oxygen-bearing species that peak at the position of the compact ridge, the emission from the HC<sub>3</sub>N isotopologue mainly distributes over the hot core, consistent with previous observations (e.g., Wright et al. 1996; Liu et al. 2002; Beuther et al. 2005). The emission of the hot core extends along the northeast–southwest direction. In addition to emission associated with the hot core, there is gas emission extending to the western IRc6 and IRc7 sources. Finally, another compact gas component is clearly detected north of the hot core. This compact component was previously revealed by emission of C<sub>2</sub>H<sub>5</sub>CN (Friedel & Snyder 2008) and CH<sub>3</sub>CN (Wang et al. 2010). We call this object HC-North, and it is denoted by an open circle in Figure 3. The combined data present that the morphology of H<sup>13</sup>CCCN  $\nu = 0$  emission is similar to that shown by ALMA data alone, but gas distribution extends to compact ridge. The intensity peaks derived from ALMA and combined data at hot core, HC-North, IRc6, and IRc7 are almost same.

Figure 4 shows sample images of HC<sub>3</sub>N  $\nu = 0$ ,  $\nu_7 = 1$ ,  $\nu_7 = 2$ ,  $\nu_6 = 1$ ,  $\nu_7 = 3$ , and  $\nu_5 = 1$  transitions, in which the combined data (red contours) are overlaid on the images of HC<sub>3</sub>N  $\nu = 0$ ,  $\nu_7 = 1$ ,  $\nu_7 = 2$  and  $\nu_7 = 3$  observed by the ALMA. We note that our IRAM observations have only covered part of HC<sub>3</sub>N transitions. We have selected unblended transitions of various excited states for the line images. The emission is integrated over different velocity ranges because the line widths are decreasing with increasing upper level energy of the transitions (see Figure 8). For the  $\nu_5 = 1$  transition, we only show the integrated emission in the narrow range  $3\text{--}7 \text{ km s}^{-1}$  in order to avoid contamination from nearby molecular lines. The images of HC<sub>3</sub>N  $\nu = 0$ ,  $\nu_7 = 1$ ,  $\nu_7 = 2$ , and  $\nu_7 = 3$  showed the gas distributions from the ALMA data and combined data have similar morphologies and peak at the same positions, but extended gas components are recovered by single dish observations. From the maps shown in Figure 4, the gas distribution of HC<sub>3</sub>N  $\nu = 0$  and HC<sub>3</sub>N  $\nu_7 = 1$  shows a “heart-shaped” structure. The “heart-shaped” structure was also observed in other low-energy molecular lines of species like CH<sub>3</sub>CN, OCS, CH<sub>3</sub>OH, C<sub>2</sub>H<sub>5</sub>CN, and NH<sub>3</sub> (Wilson et al. 2000; Friedel & Snyder 2008; Goddi et al. 2011; Zapata et al. 2011). However, the spatial distribution of higher-energy, vibrationally excited HC<sub>3</sub>N states  $\nu_7 = 2$ ,  $\nu_7 = 3$ ,  $\nu_6 = 1$  and  $\nu_5 = 1$  shows an “arc-like” ridge structure curving around Source I, which is also observed in highly excited NH<sub>3</sub> transitions (Goddi et al. 2011). The gas emission associated with the hot core, HC-North, and IRc7 is observed in all transitions with morphologies similar to that of H<sup>13</sup>CCCN

**Table 3**  
Gaussian Fits for Different  $^{13}\text{C}$  Isotopologues of  $\text{HC}_3\text{N } \nu = 0$  Toward Hot Core, HC-North, and IRc7

Molecule	Rest Frequency (GHz)	Quantum Numbers	$S_{ij}\mu^2$ (debye $^2$ )	$E_u$ (K)	Hot Core			HC-North			IRc7			Channel rms (Jy beam $^{-1}$ )
					$v_{\text{LSR}}$ (km s $^{-1}$ )	$\Delta V$ (km s $^{-1}$ )	$I_p$ (Jy beam $^{-1}$ )	$v_{\text{LSR}}$ (km s $^{-1}$ )	$\Delta V$ (km s $^{-1}$ )	$I_p$ (Jy beam $^{-1}$ )	$v_{\text{LSR}}$ (km s $^{-1}$ )	$\Delta V$ (km s $^{-1}$ )	$I_p$ (Jy beam $^{-1}$ )	
$\text{H}^{13}\text{CCCN},$ $\nu = 0$	220.39020 <sup>a</sup>	$J = 25 - 24$	348.12	137.51	...	...	...	...	...	...	...	...	...	...
	229.20310	$J = 26 - 25$	362.07	148.51	$5.73 \pm 0.01$	$8.79 \pm 0.03$	$1.01 \pm 0.01$	$4.89 \pm 0.01$	$5.98 \pm 0.02$	$0.97 \pm 0.01$	$5.53 \pm 0.04$	$7.00 \pm 0.08$	$0.32 \pm 0.01$	0.006
	238.01568 <sup>b</sup>	$J = 27 - 26$	375.96	159.93	...	...	...	$5.75 \pm 0.01$	$4.88 \pm 0.03$	$1.06 \pm 0.01$	$6.06 \pm 0.03$	$6.58 \pm 0.07$	$0.49 \pm 0.01$	0.008
$\text{HC}^{13}\text{CCN},$ $\nu = 0$	217.39857	$J = 24 - 23$	334.24	130.43	$4.43 \pm 0.01$	$7.92 \pm 0.02$	$0.99 \pm 0.01$	$4.68 \pm 0.01$	$5.63 \pm 0.02$	$0.81 \pm 0.01$	$4.11 \pm 0.02$	$6.23 \pm 0.05$	$0.39 \pm 0.01$	0.005
	226.45419	$J = 25 - 24$	348.12	141.29	$4.07 \pm 0.02$	$9.71 \pm 0.04$	$0.82 \pm 0.01$	$5.07 \pm 0.01$	$5.47 \pm 0.02$	$0.94 \pm 0.01$	$4.88 \pm 0.04$	$5.27 \pm 0.09$	$0.26 \pm 0.01$	0.006
	235.50949	$J = 26 - 25$	362.09	152.60	$5.44 \pm 0.02$	$9.22 \pm 0.04$	$0.78 \pm 0.01$	$5.44 \pm 0.01$	$5.01 \pm 0.02$	$0.97 \pm 0.01$	$6.14 \pm 0.04$	$5.25 \pm 0.08$	$0.27 \pm 0.01$	0.006
	244.56444	$J = 27 - 26$	376.03	164.33	$4.72 \pm 0.02$	$8.80 \pm 0.06$	$0.86 \pm 0.01$	$5.47 \pm 0.01$	$4.79 \pm 0.03$	$1.04 \pm 0.01$	$4.74 \pm 0.05$	$6.08 \pm 0.11$	$0.34 \pm 0.01$	0.010
$\text{HCC}^{13}\text{CN},$ $\nu = 0$	217.41957	$J = 24 - 23$	334.24	130.49	$5.41 \pm 0.01$	$9.77 \pm 0.03$	$0.86 \pm 0.01$	$5.09 \pm 0.01$	$5.04 \pm 0.02$	$0.96 \pm 0.01$	$5.58 \pm 0.03$	$5.61 \pm 0.06$	$0.31 \pm 0.01$	0.005
	226.47604	$J = 25 - 24$	348.12	141.31	$5.14 \pm 0.01$	$9.02 \pm 0.03$	$1.09 \pm 0.01$	$5.16 \pm 0.01$	$5.31 \pm 0.02$	$0.99 \pm 0.01$	$5.35 \pm 0.03$	$5.39 \pm 0.06$	$0.36 \pm 0.01$	0.006
	235.53221	$J = 26 - 25$	362.09	152.61	$6.04 \pm 0.02$	$9.40 \pm 0.04$	$0.81 \pm 0.01$	$5.26 \pm 0.01$	$4.96 \pm 0.02$	$0.95 \pm 0.01$	$5.58 \pm 0.04$	$4.64 \pm 0.08$	$0.25 \pm 0.01$	0.007
	244.58804 <sup>c</sup>	$J = 27 - 26$	376.03	164.35	...	...	...	$5.78 \pm 0.02$	$4.20 \pm 0.04$	$1.06 \pm 0.01$	...	...	...	0.014
$\text{HCCC}^{15}\text{N},$ $\nu = 0$	220.80565	25-24	348.12	127.17	$5.19 \pm 0.08$	$11.64 \pm 0.18$	$0.18 \pm 0.01$	$5.34 \pm 0.03$	$3.67 \pm 0.06$	$0.30 \pm 0.01$	$5.89 \pm 0.20$	$6.90 \pm 0.47$	$0.06 \pm 0.01$	0.006
	229.63516	26-25	362.10	137.77	$5.63 \pm 0.07$	$6.80 \pm 0.17$	$0.22 \pm 0.01$	$5.75 \pm 0.05$	$3.74 \pm 0.11$	$0.26 \pm 0.01$	$5.28 \pm 0.09$	$5.00 \pm 0.20$	$0.16 \pm 0.01$	0.009
	238.46436	27-26	376.02	148.79	$6.05 \pm 0.03$	$6.94 \pm 0.08$	$0.22 \pm 0.01$	$5.63 \pm 0.02$	$4.28 \pm 0.05$	$0.27 \pm 0.01$	$5.60 \pm 0.09$	$4.76 \pm 0.22$	$0.07 \pm 0.01$	0.004

**Notes.**<sup>a</sup> Blend with other molecular lines toward three positions.<sup>b</sup> Blend with  $\text{HC}_3\text{N } \nu_7 = 2$  at 238.01013 toward hot core.<sup>c</sup> Partial blend with other molecular lines toward hot core and IRc7.

**Table 4**  
Observed Line Parameters of HC<sub>3</sub>N and Its <sup>13</sup>C Isotopologues in all vibrationally Excited States Toward Hot Core, HC-North, and IRC7

Vib. State	Rest Frequency (GHz)	Quantum Numbers	$S_{ij}\mu^2$ (debye <sup>2</sup> )	$E_u$ (K)	Hot Core			HC-North			IRC7			Channel rms (Jy beam <sup>-1</sup> )	
					$v_{\text{LSR}}^1$ (km s <sup>-1</sup> )	$\Delta V$ (km s <sup>-1</sup> )	$I_p$ (Jy beam <sup>-1</sup> )	$v_{\text{LSR}}^1$ (km s <sup>-1</sup> )	$\Delta V$ (km s <sup>-1</sup> )	$I_p$ (Jy beam <sup>-1</sup> )	$v_{\text{LSR}}^1$ (km s <sup>-1</sup> )	$\Delta V$ (km s <sup>-1</sup> )	$I_p$ (Jy beam <sup>-1</sup> )		
					HC <sub>3</sub> N										
$v_7 = 1$	218.86080	$J = 24 - 23, l = 1e$	331.96	452.15	$5.55 \pm 0.01$	$10.83 \pm 0.01$	$4.75 \pm 0.01$	$4.44 \pm 0.01$	$7.03 \pm 0.03$	$3.23 \pm 0.01$	$4.86 \pm 0.01$	$5.44 \pm 0.02$	$1.67 \pm 0.01$	0.019	
	219.17376	$J = 24 - 23, l = 1f$	331.97	452.34	$5.07 \pm 0.01$	$9.97 \pm 0.02$	$4.83 \pm 0.01$	$4.27 \pm 0.01$	$6.42 \pm 0.03$	$3.29 \pm 0.01$	$4.97 \pm 0.02$	$5.11 \pm 0.04$	$1.65 \pm 0.01$	0.021	
	227.97728	$J = 25 - 24, l = 1e$	345.90	463.09	$5.92 \pm 0.01$	$11.19 \pm 0.01$	$5.04 \pm 0.01$	$4.58 \pm 0.01$	$7.13 \pm 0.02$	$3.51 \pm 0.01$	$5.38 \pm 0.01$	$6.85 \pm 0.03$	$1.97 \pm 0.01$	0.018	
	228.30317	$J = 25 - 24, l = 1f$	345.86	463.29	$5.20 \pm 0.01$	$9.39 \pm 0.02$	$5.15 \pm 0.01$	$4.50 \pm 0.01$	$6.71 \pm 0.02$	$3.60 \pm 0.01$	$4.93 \pm 0.02$	$5.76 \pm 0.03$	$1.88 \pm 0.01$	0.018	
	237.09338	$J = 26 - 25, l = 1e$	359.71	474.47	$5.88 \pm 0.01$	$9.68 \pm 0.02$	$4.96 \pm 0.01$	$4.65 \pm 0.01$	$7.13 \pm 0.02$	$3.48 \pm 0.01$	$5.26 \pm 0.02$	$6.01 \pm 0.04$	$1.87 \pm 0.01$	0.018	
	237.43226	$J = 26 - 25, l = 1f$	359.77	474.69	$5.45 \pm 0.01$	$8.96 \pm 0.02$	$5.24 \pm 0.01$	$4.52 \pm 0.01$	$6.72 \pm 0.02$	$3.73 \pm 0.01$	$5.49 \pm 0.02$	$4.66 \pm 0.04$	$1.90 \pm 0.01$	0.015	
	246.20915	$J = 27 - 26, l = 1e$	373.66	486.29	$6.23 \pm 0.01$	$11.36 \pm 0.02$	$5.36 \pm 0.01$	$4.67 \pm 0.02$	$6.95 \pm 0.04$	$3.55 \pm 0.02$	$5.26 \pm 0.02$	$5.20 \pm 0.04$	$2.00 \pm 0.02$	0.032	
	246.56096	$J = 27 - 26, l = 1f$	373.65	486.52	$5.82 \pm 0.01$	$10.77 \pm 0.03$	$5.31 \pm 0.01$	$4.55 \pm 0.02$	$6.97 \pm 0.05$	$3.23 \pm 0.02$	$4.97 \pm 0.02$	$5.70 \pm 0.05$	$2.28 \pm 0.02$	0.040	
$v_7 = 2$	219.67511	$J = 24 - 23, l = 0$	331.07	773.49	$5.33 \pm 0.01$	$7.50 \pm 0.02$	$1.44 \pm 0.01$	$5.22 \pm 0.01$	$4.88 \pm 0.02$	$1.23 \pm 0.01$	$6.04 \pm 0.04$	$5.07 \pm 0.08$	$0.31 \pm 0.01$	0.007	
	219.70735	$J = 24 - 23, l = 2e$	328.73	776.77	$5.60 \pm 0.01$	$8.86 \pm 0.02$	$1.57 \pm 0.01$	$5.53 \pm 0.01$	$4.96 \pm 0.02$	$1.31 \pm 0.01$	$7.26 \pm 0.03$	$7.08 \pm 0.06$	$0.60 \pm 0.01$	0.008	
	219.74187 <sup>a</sup>	$J = 24 - 23, l = 2f$	328.72	776.79	...	...	...	...	...	...	...	...	...	...	
	228.82233	$J = 25 - 24, l = 0$	344.80	784.47	$5.46 \pm 0.01$	$7.57 \pm 0.02$	$1.70 \pm 0.01$	$5.31 \pm 0.01$	$4.79 \pm 0.02$	$1.38 \pm 0.01$	$6.56 \pm 0.03$	$7.56 \pm 0.06$	$0.54 \pm 0.01$	0.007	
	228.85892	$J = 25 - 24, l = 2e$	342.67	787.76	$5.10 \pm 0.01$	$7.51 \pm 0.02$	$1.83 \pm 0.01$	$5.10 \pm 0.01$	$5.04 \pm 0.02$	$1.67 \pm 0.01$	$5.14 \pm 0.02$	$6.05 \pm 0.05$	$0.55 \pm 0.01$	0.007	
	228.89788	$J = 25 - 24, l = 2f$	342.65	787.77	$5.10 \pm 0.01$	$7.42 \pm 0.02$	$1.71 \pm 0.01$	$5.10 \pm 0.01$	$4.95 \pm 0.02$	$1.32 \pm 0.01$	$5.08 \pm 0.03$	$5.70 \pm 0.07$	$0.42 \pm 0.01$	0.008	
	237.96884	$J = 26 - 25, l = 0$	358.62	795.89	$5.28 \pm 0.01$	$7.99 \pm 0.03$	$1.83 \pm 0.01$	$5.44 \pm 0.01$	$5.10 \pm 0.03$	$1.42 \pm 0.01$	$5.07 \pm 0.03$	$6.57 \pm 0.07$	$0.64 \pm 0.01$	0.011	
	238.01013 <sup>b</sup>	$J = 26 - 25, l = 2e$	356.48	799.18	$3.50 \pm 0.01$	$11.20 \pm 0.02$	$1.63 \pm 0.01$	$5.59 \pm 0.01$	$5.60 \pm 0.01$	$1.21 \pm 0.01$	$6.08 \pm 0.03$	$3.69 \pm 0.07$	$0.23 \pm 0.01$	0.008	
	238.05390	$J = 26 - 25, l = 2f$	356.53	799.20	$5.57 \pm 0.01$	$7.33 \pm 0.01$	$1.48 \pm 0.01$	$5.68 \pm 0.01$	$4.86 \pm 0.02$	$1.37 \pm 0.01$	$6.04 \pm 0.02$	$4.00 \pm 0.05$	$0.30 \pm 0.01$	0.006	
$v_7 = 3$	220.07018 <sup>c</sup>	$J = 24 - 23, l = 1e$	330.47	1079.40	$4.68 \pm 0.14$	$9.11 \pm 0.32$	$0.31 \pm 0.01$	$6.80 \pm 0.09$	$3.26 \pm 0.22$	$0.27 \pm 0.02$	...	...	...	0.02	
	220.69969 <sup>d</sup>	$J = 24 - 23, l = 1f$	330.47	1079.78	...	...	...	...	...	...	...	...	...	...	
	229.23593	$J = 25 - 24, l = 1e$	344.29	1090.33	$6.41 \pm 0.04$	$8.87 \pm 0.08$	$0.30 \pm 0.01$	$5.85 \pm 0.03$	$4.35 \pm 0.07$	$0.24 \pm 0.01$	$5.52 \pm 0.23$	$2.65 \pm 0.54$	$0.03 \pm 0.01$	0.005	
	229.89128	$J = 25 - 24, l = 1f$	344.29	1090.74	$5.05 \pm 0.02$	$7.14 \pm 0.05$	$0.33 \pm 0.01$	$5.03 \pm 0.02$	$4.55 \pm 0.05$	$0.25 \pm 0.01$	$5.70 \pm 0.25$	$4.63 \pm 0.59$	$0.02 \pm 0.01$	0.004	
	238.40115 <sup>e</sup>	$J = 26 - 25, l = 1e$	358.11	1101.70	$5.50 \pm 0.02$	$6.34 \pm 0.05$	$0.34 \pm 0.01$	$5.54 \pm 0.03$	$4.29 \pm 0.07$	$0.21 \pm 0.01$	...	...	...	0.004	
	239.08230 <sup>f</sup>	$J = 26 - 25, l = 1f$	358.11	1102.13	$5.91 \pm 0.31$	$5.17 \pm 0.73$	$0.20 \pm 0.02$	$6.93 \pm 0.35$	$3.07 \pm 0.35$	$0.14 \pm 0.03$	...	...	...	0.04	
$v_6 = 1$	218.68256	$J = 24 - 23, l = 1e$	332.69	848.87	$5.29 \pm 0.01$	$8.56 \pm 0.03$	$1.03 \pm 0.01$	$5.39 \pm 0.01$	$5.13 \pm 0.03$	$0.85 \pm 0.01$	$5.43 \pm 0.04$	$6.20 \pm 0.08$	$0.29 \pm 0.01$	0.006	
	218.85439 <sup>g</sup>	$J = 24 - 23, l = 1f$	332.64	848.97	...	...	...	$5.88 \pm 0.03$	$5.00 \pm 0.08$	$0.89 \pm 0.01$	...	...	...	0.02	
	227.79160 <sup>h</sup>	$J = 25 - 24, l = 1e$	346.55	859.80	$6.21 \pm 0.04$	$9.08 \pm 0.09$	$1.16 \pm 0.01$	$5.75 \pm 0.03$	$5.81 \pm 0.08$	$0.96 \pm 0.01$	...	...	...	0.02	
	227.97062 <sup>i</sup>	$J = 25 - 24, l = 1f$	346.53	859.92	...	...	...	...	...	...	...	...	...	...	
	236.90036	$J = 26 - 25, l = 1e$	360.46	871.17	$5.76 \pm 0.01$	$7.57 \pm 0.02$	$1.12 \pm 0.01$	$5.52 \pm 0.01$	$5.00 \pm 0.02$	$1.09 \pm 0.01$	$6.47 \pm 0.05$	$6.08 \pm 0.12$	$0.21 \pm 0.01$	0.006	
	237.08648 <sup>j</sup>	$J = 26 - 25, l = 1f$	360.45	871.29	...	...	...	...	...	...	...	...	...	...	
	246.00874	$J = 27 - 26, l = 1e$	374.42	882.98	$5.73 \pm 0.01$	$7.66 \pm 0.03$	$1.23 \pm 0.01$	$5.74 \pm 0.01$	$4.91 \pm 0.03$	$1.13 \pm 0.01$	$6.03 \pm 0.05$	$6.96 \pm 0.11$	$0.31 \pm 0.01$	0.008	
	246.20202 <sup>k</sup>	$J = 27 - 26, l = 1f$	374.42	883.11	...	...	...	$5.69 \pm 0.01$	$5.14 \pm 0.03$	$0.97 \pm 0.01$	$6.08 \pm 0.10$	$5.60 \pm 0.24$	$0.13 \pm 0.01$	0.008	
$v_5 = 1$	218.34048	$J = 24 - 23, l = 1e$	330.47	1077.54	$6.84 \pm 0.38$	$9.33 \pm 0.90$	$0.21 \pm 0.02$	$7.62 \pm 0.18$	$7.14 \pm 0.42$	$0.40 \pm 0.02$	...	...	...	0.038	
	218.46218 <sup>l</sup>	$J = 24 - 23, l = 1f$	330.47	1077.61	...	...	...	...	...	...	...	...	...	...	
	227.43517	$J = 25 - 24, l = 1e$	344.29	1088.38	$5.80 \pm 0.14$	$8.50 \pm 0.33$	$0.39 \pm 0.01$	$6.39 \pm 0.13$	$5.79 \pm 0.30$	$0.36 \pm 0.02$	...	...	...	0.027	
	227.56196 <sup>m</sup>	$J = 25 - 24, l = 1f$	344.29	1088.46	...	...	...	...	...	...	...	...	...	...	
	236.52955	$J = 26 - 25, l = 1e$	358.11	1099.66	$5.18 \pm 0.39$	$8.04 \pm 0.91$	$0.24 \pm 0.02$	$7.28 \pm 0.18$	$6.38 \pm 0.42$	$0.46 \pm 0.03$	...	...	...	0.047	

**Table 4**  
(Continued)

Vib. State	Rest Frequency (GHz)	Quantum Numbers	$S_{ij} \mu^2$ (debye <sup>2</sup> )	$E_u$ (K)	Hot Core			HC-North			IRc7			Channel rms (Jy beam <sup>-1</sup> )
					$v_{\text{LSR}}$ (km s <sup>-1</sup> )	$\Delta V$ (km s <sup>-1</sup> )	$I_p$ (Jy beam <sup>-1</sup> )	$v_{\text{LSR}}$ (km s <sup>-1</sup> )	$\Delta V$ (km s <sup>-1</sup> )	$I_p$ (Jy beam <sup>-1</sup> )	$v_{\text{LSR}}$ (km s <sup>-1</sup> )	$\Delta V$ (km s <sup>-1</sup> )	$I_p$ (Jy beam <sup>-1</sup> )	
$v_4 = 1$	236.66141	$J = 26 - 25, l = 1f$	358.11	1099.75	4.40 ± 0.06	9.84 ± 0.14	0.30 ± 0.01	5.59 ± 0.05	4.60 ± 0.12	0.24 ± 0.01	...	...	...	0.008
	245.62361	$J = 27 - 26, l = 1e$	371.92	1111.37	6.51 ± 0.47	9.48 ± 1.09	0.27 ± 0.03	6.60 ± 0.32	7.10 ± 0.75	0.33 ± 0.03	...	...	...	0.058
	245.76049	$J = 27 - 26, l = 1f$	371.92	1111.46	6.38 ± 0.07	8.92 ± 0.17	0.34 ± 0.01	5.88 ± 0.06	4.81 ± 0.13	0.32 ± 0.01	...	...	...	0.012
	218.02178 <sup>a</sup>	24 - 23	322.18	1376.38	...	...	...	4.02 ± 0.09	4.23 ± 0.21	0.09 ± 0.01	...	...	...	0.006
	227.10310 <sup>o</sup>	25 - 24	335.60	1387.27	4.96 ± 0.18	3.14 ± 0.41	0.10 ± 0.01	6.01 ± 0.32	2.18 ± 0.73	0.05 ± 0.01	...	...	...	0.014
	236.18406 <sup>p</sup>	26 - 25	349.02	1398.61	7.00 ± 0.17	3.40 ± 0.40	0.12 ± 0.01	...	...	...	...	...	...	0.016
245.26463 <sup>o</sup>	27 - 26	362.42	1410.38	7.67 ± 0.05	7.91 ± 0.12	0.23 ± 0.01	6.23 ± 0.15	3.30 ± 0.35	0.05 ± 0.01	...	...	...	0.006	
$v_7 = 1$	H <sup>13</sup> CCCN													
	220.93814 <sup>q</sup>	$J = 25 - 24, l = 1e$	345.90	456.03	7.64 ± 0.07	10.43 ± 0.17	0.15 ± 0.01	5.37 ± 0.04	3.93 ± 0.08	0.19 ± 0.01	...	...	...	0.005
	221.24624 <sup>r</sup>	$J = 25 - 24, l = 1f$	345.87	456.22	...	...	...	...	...	...	...	...	...	...
	229.77288 <sup>s</sup>	$J = 26 - 25, l = 1e$	359.71	467.06	8.44 ± 0.07	12.57 ± 0.17	0.13 ± 0.01	5.86 ± 0.03	4.19 ± 0.08	0.18 ± 0.01	...	...	...	0.004
	230.09322 <sup>t</sup>	$J = 26 - 25, l = 1f$	359.78	467.27	...	...	...	...	...	...	...	...	...	...
	238.60729 <sup>u</sup>	$J = 27 - 26, l = 1e$	373.64	478.51	1.78 ± 0.06	7.87 ± 0.14	0.13 ± 0.01	6.16 ± 0.05	2.64 ± 0.11	0.10 ± 0.01	...	...	...	0.004
	238.93987 <sup>v</sup>	$J = 27 - 26, l = 1f$	373.64	478.73	...	...	...	5.89 ± 0.07	2.90 ± 0.16	0.13 ± 0.01	...	...	...	0.007
	221.76012 <sup>w</sup>	$J = 25 - 24, l = 0$	344.83	774.34	...	...	...	5.98 ± 0.20	1.95 ± 0.43	0.03 ± 0.01	...	...	...	0.007
	221.82558 <sup>x</sup>	$J = 25 - 24, l = 2f$	342.61	777.76	4.14 ± 0.09	3.06 ± 0.21	0.05 ± 0.01	4.42 ± 0.18	1.71 ± 0.54	0.02 ± 0.01	...	...	...	0.004
	239.48875 <sup>y</sup>	$J = 27 - 26, l = 0$	372.43	796.90	7.92 ± 0.09	2.63 ± 0.22	0.05 ± 0.01	...	...	...	...	...	...	0.004
239.57131 <sup>z</sup>	$J = 27 - 26, l = 2f$	370.34	800.33	...	...	...	4.96 ± 0.13	4.01 ± 0.31	0.04 ± 0.01	...	...	...	0.004	
$v_7 = 1$	HC <sup>13</sup> CCN													
	217.91300	$J = 24 - 23, l = 1e$	331.99	446.62	7.49 ± 0.10	9.91 ± 0.23	0.11 ± 0.01	5.84 ± 0.04	3.76 ± 0.10	0.17 ± 0.01	6.02 ± 0.19	2.88 ± 0.44	0.03 ± 0.01	0.005
	236.06663 <sup>aa</sup>	$J = 26 - 25, l = 1e$	359.72	468.84	...	...	...	7.06 ± 0.14	6.27 ± 0.32	0.18 ± 0.01	...	...	...	0.014
	245.14293 <sup>ab</sup>	$J = 27 - 26, l = 1e$	373.60	480.61	...	...	...	4.96 ± 0.07	4.86 ± 0.17	0.15 ± 0.01	...	...	...	0.007
	245.49675 <sup>ab</sup>	$J = 27 - 26, l = 1f$	373.67	480.85	...	...	...	5.74 ± 0.07	4.64 ± 0.16	0.14 ± 0.01	...	...	...	0.006
	227.85096 <sup>ac</sup>	$J = 25 - 24, l = 2e$	342.65	776.61	...	...	...	...	...	...	...	...	...	...
	236.91647 <sup>ad</sup>	$J = 26 - 25, l = 0$	358.62	784.96	5.54 ± 0.48	5.87 ± 1.13	0.09 ± 0.02	...	...	...	7.40 ± 0.49	4.00 ± 1.16	0.07 ± 0.02	0.026
	236.96188 <sup>ac</sup>	$J = 26 - 25, l = 2e$	356.48	787.98	...	...	...	...	...	...	...	...	...	...
	237.01002	$J = 26 - 25, l = 2f$	356.52	787.99	7.66 ± 0.17	4.28 ± 0.40	0.06 ± 0.01	7.09 ± 0.16	5.33 ± 0.38	0.04 ± 0.01	7.50 ± 0.19	3.80 ± 0.32	0.04 ± 0.01	0.004
	246.02146	$J = 27 - 26, l = 0$	372.43	796.76	5.92 ± 0.19	2.38 ± 0.45	0.04 ± 0.01	6.90 ± 0.25	2.01 ± 0.55	0.03 ± 0.01	5.30 ± 0.14	2.95 ± 0.32	0.06 ± 0.07	0.007
246.12624 <sup>af</sup>	$J = 27 - 26, l = 2f$	370.41	799.81	...	...	...	4.55 ± 0.40	1.77 ± 1.17	0.02 ± 0.01	5.73 ± 0.25	3.31 ± 0.59	0.03 ± 0.01	0.005	
$v_7 = 1$	HCC <sup>13</sup> CN													
	217.94317	$J = 24 - 23, l = 1e$	331.99	446.02	6.24 ± 0.13	6.58 ± 0.30	0.08 ± 0.01	6.11 ± 0.06	4.13 ± 0.13	0.15 ± 0.01	7.94 ± 0.21	2.94 ± 0.49	0.03 ± 0.01	0.006
	218.25564	$J = 24 - 23, l = 1f$	332.01	446.23	5.09 ± 0.08	8.10 ± 0.19	0.10 ± 0.01	5.74 ± 0.04	3.31 ± 0.10	0.12 ± 0.01	6.07 ± 0.27	1.57 ± 0.47	0.02 ± 0.01	0.004
	236.09931	$J = 26 - 25, l = 1e$	359.72	468.12	5.61 ± 0.12	6.49 ± 0.27	0.10 ± 0.01	5.46 ± 0.07	5.05 ± 0.15	0.17 ± 0.01	4.85 ± 0.21	2.18 ± 0.48	0.03 ± 0.01	0.007
	236.43766	$J = 26 - 25, l = 1f$	359.77	468.35	5.89 ± 0.20	5.94 ± 0.47	0.11 ± 0.01	6.00 ± 0.12	3.54 ± 0.27	0.15 ± 0.01	6.02 ± 0.22	3.68 ± 0.52	0.04 ± 0.01	0.013
	245.17687 <sup>ag</sup>	$J = 26 - 25, l = 1e$	373.61	479.82	...	...	...	5.60 ± 0.07	3.58 ± 0.18	0.16 ± 0.01	...	...	...	0.009
245.52814 <sup>ah</sup>	$J = 26 - 25, l = 1f$	373.59	480.04	...	...	...	6.24 ± 0.17	3.27 ± 0.40	0.15 ± 0.02	...	...	...	0.02	
$v_7 = 2$	218.81231	$J = 24 - 23, l = 2f$	328.70	764.46	5.98 ± 0.18	6.12 ± 0.23	0.09 ± 0.01	6.78 ± 0.15	5.46 ± 0.34	0.04 ± 0.01	4.26 ± 0.12	2.67 ± 0.28	0.04 ± 0.01	0.004

**Table 4**  
(Continued)

Vib. State	Rest Frequency (GHz)	Quantum Numbers	$S_{ij} \mu^2$ (debye <sup>2</sup> )	$E_u$ (K)	Hot Core			HC-North			IRc7			Channel rms (Jy beam <sup>-1</sup> )
					$v_{\text{LSR}}$ (km s <sup>-1</sup> )	$\Delta V$ (km s <sup>-1</sup> )	$I_p$ (Jy beam <sup>-1</sup> )	$v_{\text{LSR}}$ (km s <sup>-1</sup> )	$\Delta V$ (km s <sup>-1</sup> )	$I_p$ (Jy beam <sup>-1</sup> )	$v_{\text{LSR}}$ (km s <sup>-1</sup> )	$\Delta V$ (km s <sup>-1</sup> )	$I_p$ (Jy beam <sup>-1</sup> )	
	227.85148 <sup>ai</sup>	$J = 25 - 24, l = 0$	344.83	772.21	...	...	...	...	...	...	...	...	...	...
	236.95904 <sup>aj</sup>	$J = 26 - 25, l = 0$	358.60	783.50	...	...	...	...	...	...	...	...	...	...
	237.00158 <sup>ak</sup>	$J = 26 - 25, l = 2e$	356.53	786.61	9.42 ± 0.11	5.75 ± 0.26	0.06 ± 0.01	6.21 ± 0.16	3.67 ± 0.37	0.03 ± 0.01	...	...	...	0.004
	246.16464	$J = 27 - 26, l = 2f$	370.38	798.36	4.96 ± 0.31	4.75 ± 0.72	0.04 ± 0.01	6.00 ± 1.30	2.16 ± 1.27	0.02 ± 0.01	7.97 ± 0.19	3.83 ± 0.45	0.06 ± 0.01	0.008

**Notes.**

- <sup>a</sup> Blend with HNCO  $v = 0$  at 219.73719 GHz toward three positions.  
<sup>b</sup> Blend with H<sup>13</sup>CCCN  $v = 0$  at 238.01568 GHz toward hot core.  
<sup>c</sup> Blend with other molecular lines toward IRc7.  
<sup>d</sup> Blend with other molecular lines toward three positions.  
<sup>e</sup> Blend with other molecular lines toward IRc7.  
<sup>f</sup> Blend with other molecular lines toward IRc7.  
<sup>g</sup> Blend with HC<sub>3</sub>N  $v_7 = 1$  at 218.86080 GHz toward hot core and IRc7.  
<sup>h</sup> Blend with C<sub>2</sub>H<sub>5</sub>CN at 227.78097 GHz toward IRc7.  
<sup>i</sup> Blend with HC<sub>3</sub>N  $v_7 = 1$  at 227.97728 GHz and C<sub>2</sub>H<sub>3</sub>CN at 227.96759 GHz toward hot core, HC-North, and IRc7.  
<sup>j</sup> Blend with HC<sub>3</sub>N  $v_7 = 1$  at 237.09338 GHz toward three positions.  
<sup>k</sup> Blend with HC<sub>3</sub>N  $v_7 = 1$  at 246.20915 GHz toward hot core.  
<sup>l</sup> Blend with C<sub>2</sub>H<sub>3</sub>CN at 218.46374 GHz toward three positions.  
<sup>m</sup> Blend with CH<sub>3</sub>OCHO at 227.56173 GHz toward three positions.  
<sup>n</sup> Blend with other molecular lines toward hot core and IRc7.  
<sup>o</sup> Partial blend with other molecular lines toward IRc7.  
<sup>p</sup> Blend with other molecular lines toward HC-North and IRc7.  
<sup>q</sup> Blend with other molecular lines toward IRc7.  
<sup>r</sup> Blend with other molecular lines toward hot core and HC-North, next to the strong line toward IRc7.  
<sup>s</sup> Blend with other molecular lines toward IRc7.  
<sup>t</sup> Blend with CH<sub>2</sub>CHCN  $v_{15} = 1$  at 230.09289 GHz toward three positions.  
<sup>u</sup> Not detected toward IRc7.  
<sup>v</sup> Blend with CH<sub>3</sub><sup>13</sup>CN at 238.94631 GHz toward hot core, not detected toward IRc7.  
<sup>w</sup> Blend with other molecular lines toward hot core and IRc7.  
<sup>x</sup> Blend with other molecular lines toward IRc7.  
<sup>y</sup> Not detected toward HC-North and IRc7.  
<sup>z</sup> Blend with other molecular lines toward hot core and IRc7.  
<sup>aa</sup> Blend with other molecular lines toward hot core and IRc7.  
<sup>ab</sup> Blend with U-lines toward hot core and IRc7.  
<sup>ac</sup> Blend with HCC<sup>13</sup>CN  $v_7 = 2$  at 227.85148 GHz toward three positions.  
<sup>ad</sup> Line intensities  $< 3\sigma$  toward HC-North.  
<sup>ae</sup> Blend with HCC<sup>13</sup>CN  $v_7 = 2$  at 236.95904 GHz toward three positions.  
<sup>af</sup> Next to the strong lines toward hot core.  
<sup>ag</sup> Blend with other molecular lines toward hot core and IRc7.  
<sup>ah</sup> Blend with other molecular lines toward hot core and IRc7.  
<sup>ai</sup> Blend with HC<sup>13</sup>CCN  $v_7 = 2$  at 227.85096 GHz toward three positions.  
<sup>aj</sup> Blend with HC<sup>13</sup>CCN  $v_7 = 2$  at 236.96188 GHz toward three positions.  
<sup>ak</sup> Next to the strong lines toward IRc7.

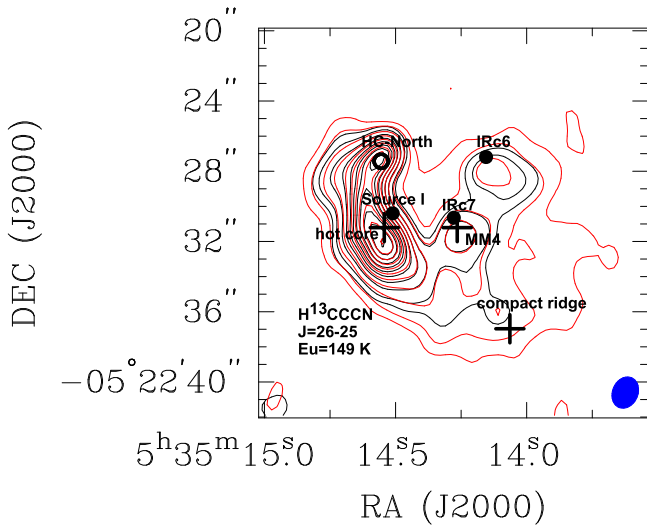


**Figure 3.** Velocity integrated intensity maps of  $\text{H}^{13}\text{CCCN } \nu = 0$  from the combined ALMA+IRAM 30 m data (red contours) and ALMA data (black contours). In each panel, the synthesized beam is shown in the bottom right corner. The contour levels are 5%, 10%, 20%, 30%, 40%, 50%, 60%, 70%, 80%, 90%, and 99% of the emission peak of  $9.7 \text{ Jy beam}^{-1} \text{ km s}^{-1}$ . The cross symbols mark the continuum peak positions of hot core, compact ridge, and MMA. The HC-North component is denoted by an open circle. The solid circles indicate radio Source I and infrared sources IRc6 and IRc7.

$\nu = 0$ . Strikingly, the emission of  $\text{HC}_3\text{N}$  lines with different upper level energies peaks at different positions. The emission peak of  $\text{HC}_3\text{N } \nu = 0$  is located south of the hot core continuum peak, whereas the highly excited  $\text{HC}_3\text{N } \nu_5 = 1$  emission peak is to the northeast of the hot core continuum peak. By choosing all unblended lines in each state ( $\text{HC}_3\text{N } \nu = 0, \nu_7 = 1, \nu_7 = 2, \nu_6 = 1, \nu_7 = 3, \text{ and } \nu_5 = 1$ ), we draw a map of the peak position as a function of upper level energy  $E_u$  toward three positions, showing that all transitions in the same excited state have similar locations for the emission peak. This is shown in Figure 5, where we can see that the peak position along RA.Offset and DEC.Offset directions are increasing as  $E_u$  increases. This means that the line emission peak moves gradually from the south to the northeast as upper-level energies increase.

The results show that the morphologies of  $\text{HC}_3\text{N}$  gas emission with ALMA are similar to those from combined data, and the images of combined data are more extended than those from ALMA data alone (see Figures 3 and 4), but the gas emissions of both ALMA and combined data peak at the same positions. One can also see that spectral profiles of vibrationally excited  $\text{HC}_3\text{N}$  transitions extracted from ALMA and combined data are almost the same and have almost identical peak intensity (see Figure 2). Therefore, one can safely use vibrationally excited  $\text{HC}_3\text{N}$  transitions to derive excitation gradients. The derived excitation gradients are robust and not subject to sampling problems.

### 3.3. Line Kinematics

Figure 6 shows the line profiles of selected transitions from the ALMA data:  $\text{HCCC}^{15}\text{N } \nu = 0$  ( $J = 27-26$ ),  $\text{HC}^{13}\text{CCN } \nu = 0$  ( $J = 27-26$ ),  $\text{HC}_3\text{N } \nu_7 = 1$  ( $J = 25-24, l = 1f$ ),  $\nu_7 = 2$  ( $J = 24-23, l = 0$ ), and  $\nu_7 = 3$  ( $J = 25-24, l = 1f$ ), toward the positions of the hot core, HC-North, and IRc7. At each position, line profiles from different vibrational states are similar, with broader line widths toward the hot core than the

other positions. The central velocities of molecular lines at the three positions are essentially the same, ranging from 5 to  $8 \text{ km s}^{-1}$ . In general, all transitions have emission intensities weaker toward IRc7 than toward the hot core and HC-North. Although  $\text{HC}_3\text{N } \nu_7 = 2$ ,  $\text{HC}_3\text{N } \nu_7 = 3$ ,  $\text{HC}^{13}\text{CCN } \nu = 0$ , and  $\text{HCCC}^{15}\text{N } \nu = 0$  have comparable intensities toward the hot core and HC-North,  $\text{HC}_3\text{N } \nu_7 = 1$  is weaker toward HC-North. In addition, the line profiles of  $\text{HC}_3\text{N } \nu_7 = 1$  from HC-North and IRc7 show significant blue wings, indicating different kinematics.

## 4. Discussion

### 4.1. Properties of Hot Core, HC-North and IRc7

Recent high spatial resolution observations threw doubt on a possible spatial segregation between nitrogen- and oxygen-bearing molecules, with a possible “chemical differentiation” in the Orion KL region suggesting that nitrogen- and oxygen-bearing molecules may arise not only from the hot core and compact ridge, but also from multiple components (e.g., Friedel & Snyder 2008; Widicus Weaver & Friedel 2012). Nitrogen-bearing molecules like  $\text{C}_2\text{H}_5\text{CN}$  and  $\text{C}_2\text{H}_3\text{CN}$  are clearly observed toward IRc7, and not only in the hot core (e.g., Friedel & Snyder 2008; Widicus Weaver & Friedel 2012). However, previous images were made from single lower-energy transitions for certain species. Low-energy transitions may sample the emission from both hot and cold gas components, whereas highly excited transitions are expected to come only from hot gas environments. Therefore, the ALMA observations presented here with a better image fidelity and sensitivity are well-suited to study the spatial distribution of highly excited molecular transitions.

The ALMA observations of  $\text{HC}_3\text{N}$  vibrational transitions covering a broad range of upper-level energies (452–1111 K) should give a better insight into the spatial distribution of nitrogen-bearing molecules. From Figures 3 and 4, the emission of  $\text{HC}_3\text{N}$  vibrationally excited transitions mainly distributes over multiple spatial components near the hot core, but not in the compact ridge. Strong emission is observed toward the hot core, and IRc7 is detected in all the  $\text{HC}_3\text{N}$  vibrational transitions. Another gas component located north of the hot core (namely HC-North, denoted by an open circle symbol in Figure 3) is detected. HC-North has been marginally detected in lower-energy  $\text{C}_2\text{H}_5\text{CN}$  transitions (Friedel & Snyder 2008). The intensity peaks of  $\text{HC}_3\text{N}$  vibrational lines at IRc7 do not seem to change with the upper-level energy (see Figure 5). The intensity peak at HC-North moves from the southeast to northwest with increasing  $E_u$ . The intensity peak associated with the hot core moves from the south to the northeast as the upper-level energy increases. As shown in Table 1, the hot core is the position (among the three studied in this work) with the highest rotational temperature and column density.

Out of the three positions studied in this work, the hot core and IRc7 clearly show the largest number of molecular lines. N-bearing (weak) lines are less blended toward HC-North (see Figure 2, Tables 3 and 4). A multi-transition study shows that the central velocities at the three positions are in the range between  $5-8 \text{ km s}^{-1}$  (see Figure 6). Note that the  $\text{HC}_3\text{N } \nu_7 = 1$  spectra toward HC-North and IRc7 show significant blue wings. Figure 7 presents line width as a function of upper-level energy. The values of line widths are obtained from Gaussian

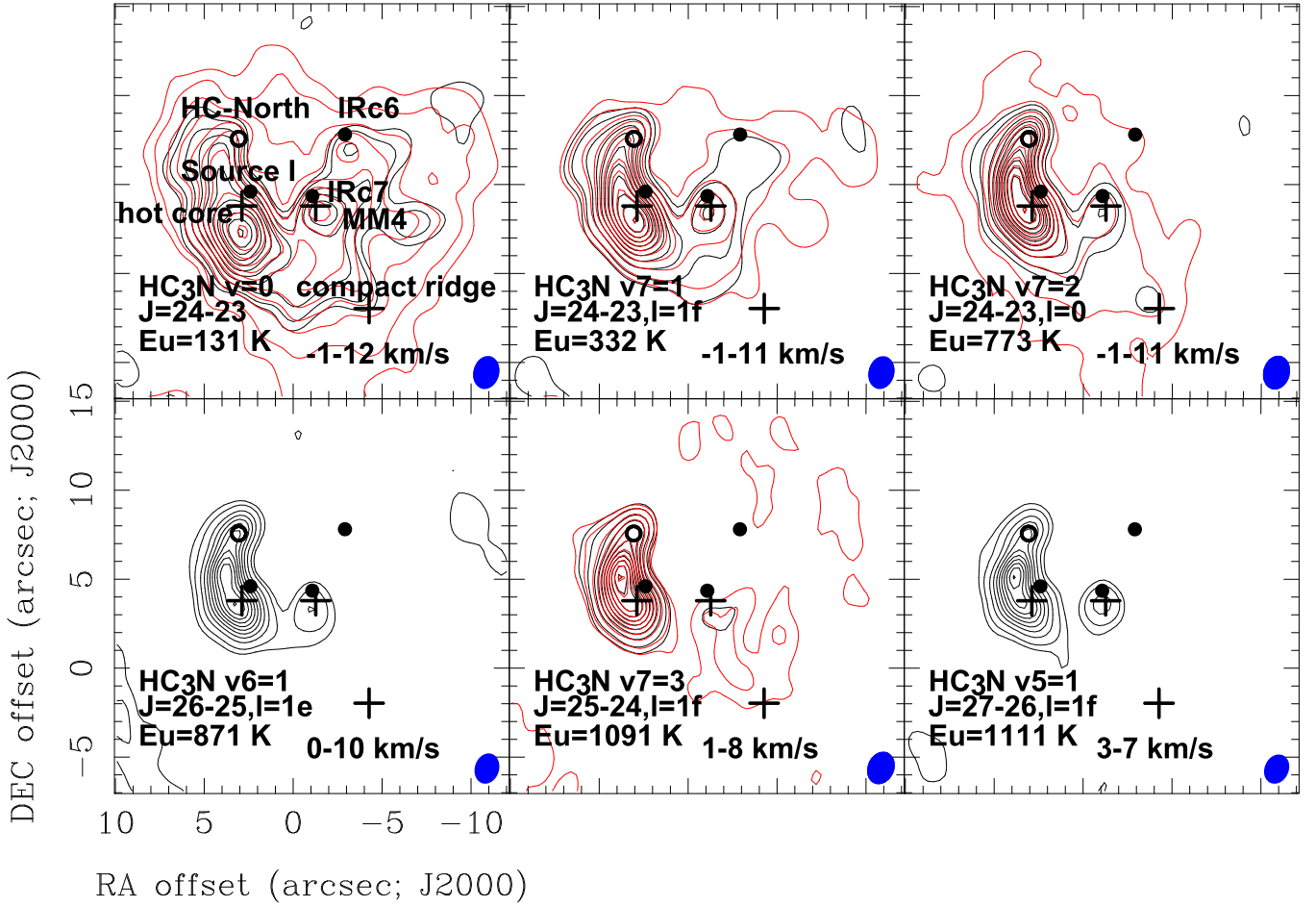


**Figure 4.** Velocity integrated intensity maps of  $\text{HC}_3\text{N } v=0$ ,  $\text{HC}_3\text{N } v_7=1$ ,  $\text{HC}_3\text{N } v_7=2$ ,  $\text{HC}_3\text{N } v_6=1$ ,  $\text{HC}_3\text{N } v_7=3$ , and  $\text{HC}_3\text{N } v_5=1$  from the combined ALMA +IRAM 30 m data (red contours) and ALMA data (black contours). For each species, the integral velocity range is shown in each map. The contour levels are 5%, 10%, 20%, 30%, 40%, 50%, 60%, 70%, 80%, 90%, and 99% of the emission peak. The emission peaks of  $\text{HC}_3\text{N } v=0$ ,  $\text{HC}_3\text{N } v_7=1$ ,  $\text{HC}^{13}\text{CCN } v_7=1$ ,  $\text{H}^{13}\text{CCCN } v_7=1$ ,  $\text{HC}_3\text{N } v_7=2$ ,  $\text{HC}^{13}\text{CCN } v_7=2$ ,  $\text{HC}_3\text{N } v_6=1$ ,  $\text{HC}_3\text{N } v_7=3$ , and  $\text{HC}_3\text{N } v_5=1$  are 68.4, 53.0, 12.1, 10.3, 3.1, and 2.7  $\text{Jy beam}^{-1} \text{ km s}^{-1}$ , respectively. The cross and circle symbols have same meaning as in Figure 3. The origin of the offset position is R.A.(J2000) =  $05^{\text{h}}35^{\text{m}}14^{\text{s}}35$  and decl.(J2000) =  $-05^{\circ}22'35''00$ .

fits of  $\text{HC}_3\text{N } v_7=1$ ,  $v_7=2$ ,  $v_7=3$ ,  $v_6=1$ ,  $v_5=1$ , and  $v_4=1$  vibrational lines. Note that the data from  $\text{HC}_3\text{N } v_5=1$  and  $v_4=1$  vibrational lines toward IRc7 are not included in the plot due to line-blending problems. Line widths decrease with increasing upper-level energy of the transitions. One can also see that the line width is broadest in the hot core and narrowest in HC-North (see Figures 6 and 7).

#### 4.2. Vibrationally Excited States of $\text{HC}_3\text{N}$ in the Hot Core

Only a few transitions of  $\text{HC}_3\text{N}$  in  $v_7=1$ ,  $v_7=2$ ,  $v_6=1$ , and  $v_5=1$  states were detected toward Orion KL in previous lower spatial resolution observations (Clark et al. 1976; Goldsmith et al. 1982, 1983, 1985; Schilke et al. 1997; de Vicente et al. 2002). In addition, the line emission of these vibrationally excited transitions suffers from beam dilution in the low spatial resolution observation, and cannot provide accurate spatial information because these lines mainly populate at small scales. Therefore, the physical conditions and emission origin traced by these highly excited lines is not well-constrained. The ALMA observations have resolved the hot core, HC-North and IRc7 sources, and allowed us to detect  $\text{HC}_3\text{N}$  in seven vibrational states ( $v_7=1$ ,  $v_7=2$ ,  $v_6=1$ ,  $v_7=3$ ,  $v_5=1$ ,  $v_4=1$ , and  $v_4=v_7=1$ ) and its three

isotopologues ( $\text{H}^{13}\text{CCCN}$ ,  $\text{HC}^{13}\text{CCN}$  and  $\text{HCC}^{13}\text{CN}$ ) in  $v_7=1$  and  $v_7=2$  toward the three positions.

Based on the detection of multiple transitions, we have calculated rotational temperatures and column densities for each vibrationally excited state using XCLASS. In Figure 8, we plot the derived rotational temperature and column density for each vibrationally excited state as a function of corresponding vibrational energy level. Note that the parameters of the  $\text{HC}_3\text{N } v_5=1$  and  $v_4=1$  vibrational lines toward IRc7 are not included in the plot due to line-blending problems. Toward the three positions, the derived rotational temperatures of vibrationally excited states increase with increasing vibrational energy level (see top panel of Figure 8). However, lower column densities are derived from higher-energy lines compared to lower-energy transitions (see bottom panel of Figure 8). Note that  $\text{HC}_3\text{N } v_5=1$  and  $v_7=3$  with  $E_u < 1700$  K have almost the same rotational temperature and column density. The level diagram shows that both  $\text{HC}_3\text{N } v_5=1$  and  $v_7=3$  (see Figure 1 of Wyrowski et al. 1999) lie on a nearly equal energy level and should have almost equal line profiles and excited temperatures. We take the hot core position as an example to expound rotational temperature differences among these vibrationally excited states. Vibrational excitation temperatures of  $184 \pm 13$  K,  $198 \pm 8$  K and  $209 \pm 14$  K for

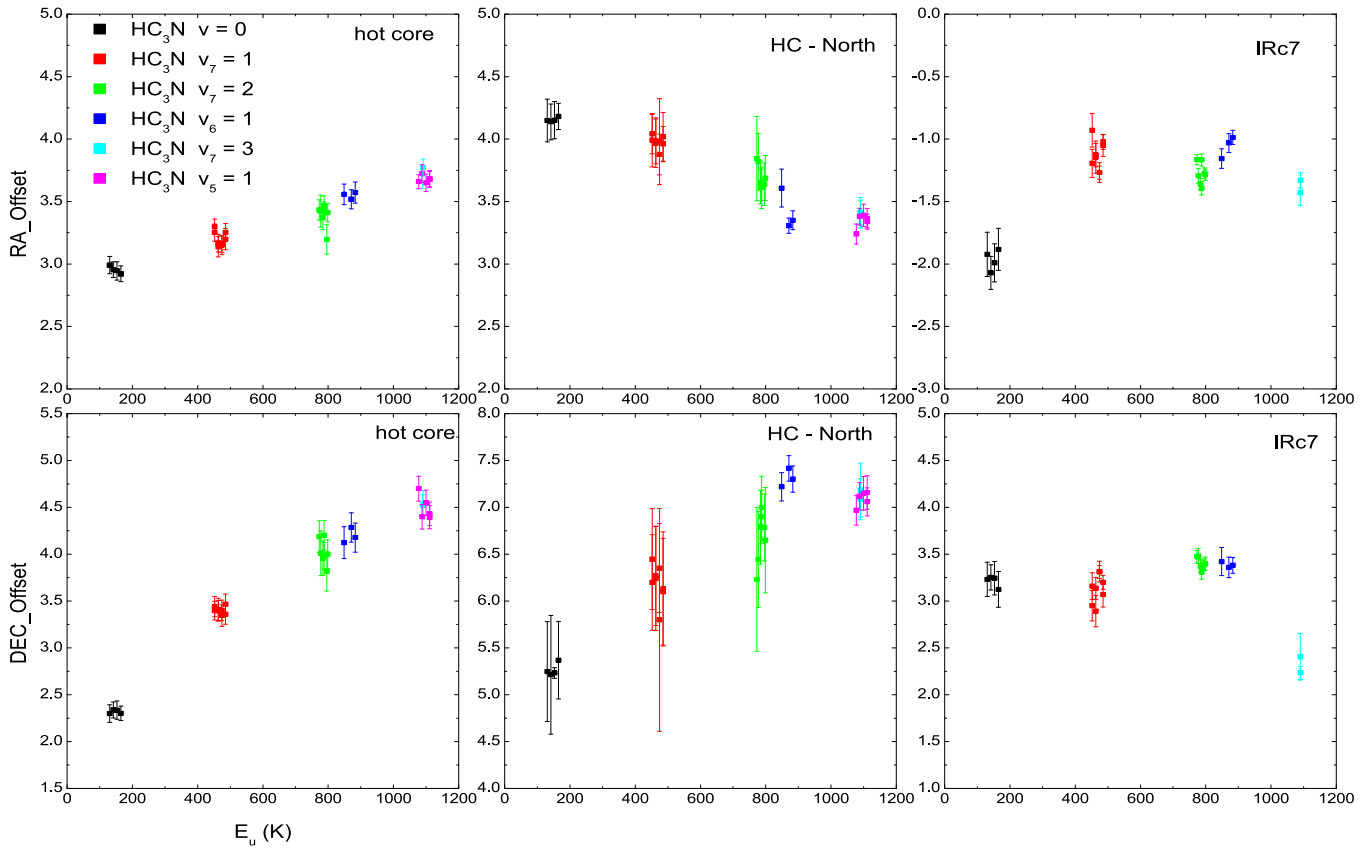


**Figure 5.** Plot of the peak position along RA\_Offset and DEC\_Offset as a function of the upper-level energy of unblending lines toward three positions. The origin of the offset position is R.A.(J2000) = 05<sup>h</sup>35<sup>m</sup>14<sup>s</sup>.35 and decl.(J2000) = -05°22′35″00.

HC<sub>3</sub>N  $v_7 = 1$ ,  $v_7 = 2$ , and  $v_6 = 1$  are derived. Previous observations showed that the three states were described by a single temperature of 150 K (Goldsmith et al. 1982, 1983, 1985). The excitation temperature of  $v_5 = 1$  is  $237 \pm 12$  K, which agrees well with the temperature of  $>230$  K for  $v_5 = 1$  derived from PdBI observations (de Vicente et al. 2002). Even higher excited states (e.g.,  $v_4 = 1$ ) have a higher excitation temperature of  $321 \pm 78$  K.

#### 4.3. Vibrational Temperature

One important technique to derive the rotation temperature and column density from molecular line emission is the “rotational temperature diagram.” Under the LTE assumption, the population of a certain energy level will follow the Boltzmann distribution. Under the assumptions of gas being optically thin and gas emission filling the beam, the natural logarithm of  $N_u/g_u$  versus the energy of the upper-level  $E_u$  follows a straight line with slope  $1/T$  (Goldsmith & Langer 1999; Liu et al. 2002; Remijan et al. 2003). We fitted multiple transitions by using the least-squares method. The rotational temperature diagram for the observed HC<sub>3</sub>N lines from the hot core is shown in Figure 9. The data include  $v_7 = 1$ ,  $v_7 = 2$ ,  $v_7 = 3$ ,  $v_6 = 1$ , and  $v_5 = 1$ , for which more than three transitions have been detected. The rotation diagram gives an excitation temperature of  $210 \pm 5$  K for all the 29 vibrationally excited HC<sub>3</sub>N lines, whereas for all the vibrationally excited HC<sub>3</sub>N lines with same  $J = 24-23$ , we obtain a similar temperature of  $220 \pm 15$  K.

#### 4.4. Heating Mechanism: Internal versus External

The heating mechanism in hot cores has been under debate in the last years. Two main heating mechanisms have been proposed: (i) the core is heated internally by an embedded luminous protostar (e.g., Masson & Mundy 1988; Kaufman et al. 1998; de Vicente et al. 2002) or (ii) externally illuminated and heated by nearby protostars (e.g., Menten & Reid 1995; Wright et al. 1996; Gezari et al. 1998; Wilson et al. 2000). Alternatively, shocks can also increase the temperature, resulting in the rich chemistry observed in hot cores (e.g., Palau et al. 2011; Zapata et al. 2011).

The study of different transitions for a given species provides us insight into the different physical properties and kinematics for the Orion KL objects, because these transitions require different excitation conditions. As stated in Section 3.2, the intensity peak of HC<sub>3</sub>N  $v = 0$  with  $E_u < 170$  K is located southeast of Source I (see Figure 4). The intensity peaks of moderate excited transitions of HC<sub>3</sub>N  $v_7 = 1$  and  $v_7 = 2$  are located southeast of Source I and close to the continuum peak of the hot core, whereas HC<sub>3</sub>N  $v_7 = 3$  and  $v_5 = 1$ , which have higher upper-level energies ( $E_u > 1077$  K) and require higher excitation temperatures of  $237 \pm 10$  K and  $237 \pm 12$  K, respectively, have their intensity peaks located northeast of Source I. Our LTE calculations suggest that the excitation temperature is increasing and column density decreasing as  $E_u$  rises (see Figure 8).

If the hot core is internally heated and there was a single massive protostellar source in the hot core, one may expect that the hottest molecular gas peaks there. However, observations in radio, millimeter, and infrared wavelengths suggest that there is

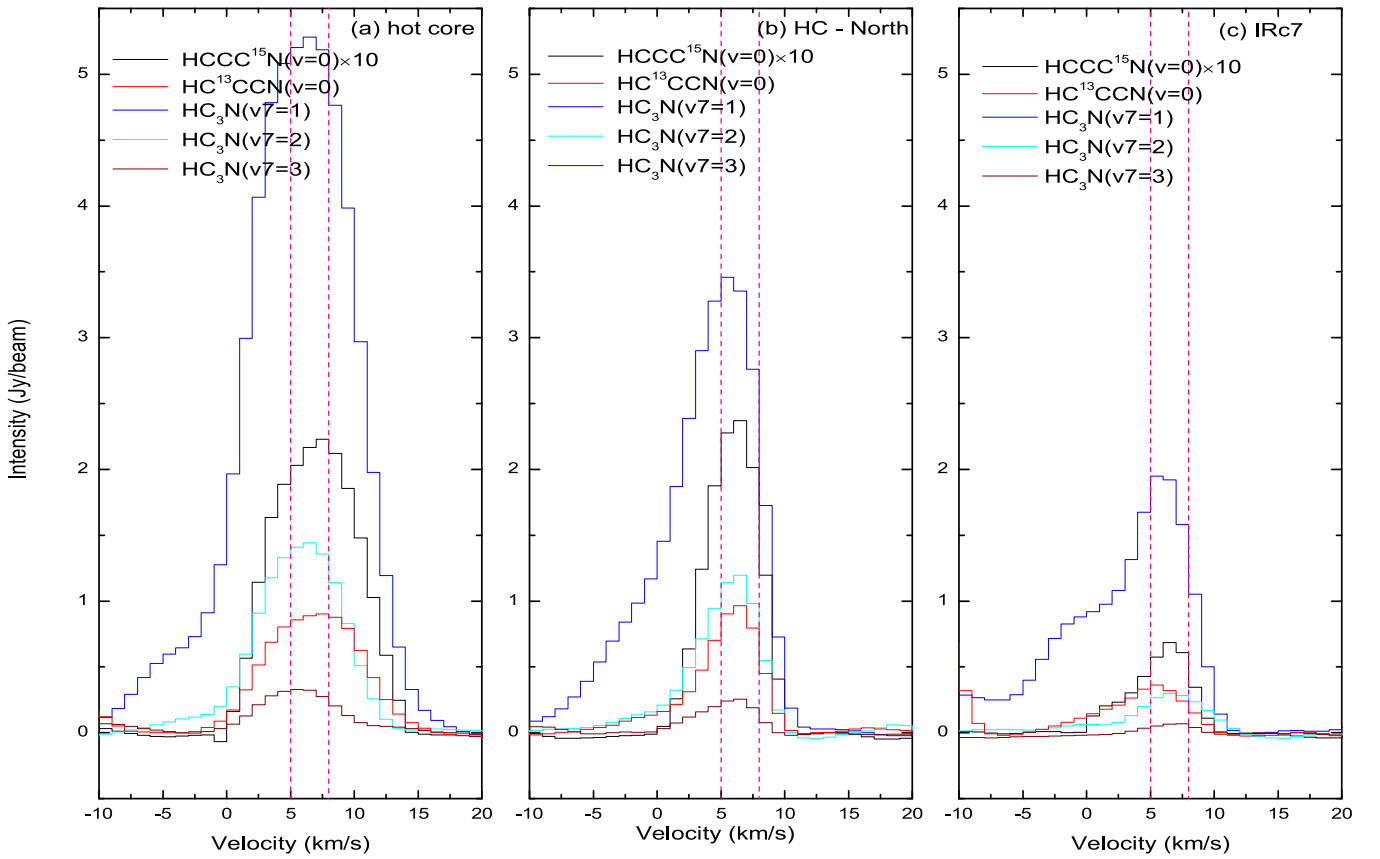


**Figure 6.** Representative spectra at hot core, HC-North, and IRc7 positions:  $\text{HCCC}^{15}\text{N } v = 0$  at 238.46436 GHz,  $\text{HC}^{13}\text{CCN } v = 0$  at 244.56444 GHz,  $\text{HC}_3\text{N } v_7 = 1$  at 228.30317 GHz,  $\text{HC}_3\text{N } v_7 = 2$  at 219.67511 GHz, and  $\text{HC}_3\text{N } v_7 = 3$  at 229.89128 GHz. Two pink lines denote the velocity of  $5 \text{ km s}^{-1}$  and  $8 \text{ km s}^{-1}$ , respectively.

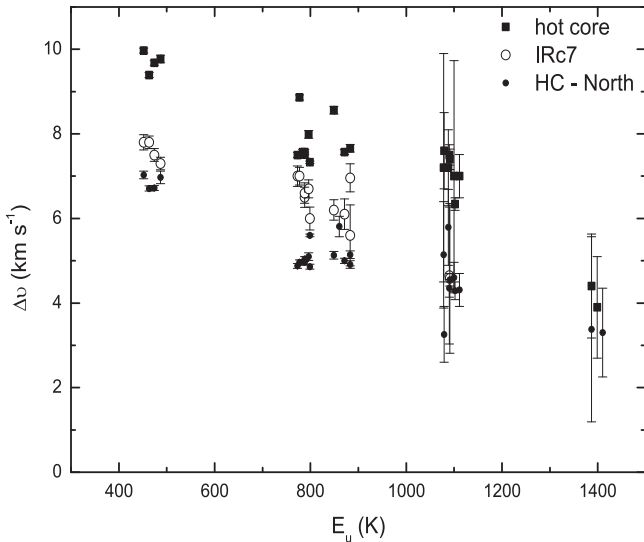


**Figure 7.** Plot of line widths as a function of upper-level energies ( $E_u$ ). The square, solid circle, and open circle denote the line widths derived from hot core, HC-North, and IRc7 positions, respectively.

no a single massive protostellar source in the hot core (Menten & Reid 1995; Greenhill et al. 2004; Friedel & Snyder 2008). We also find that the molecular gas at the center has lower gas temperature and higher column density, and the intensity peaks move from southeast to northeast of Source I with increasing  $E_u$  (see Figure 5). Our results appear to not support internal heating in the Orion KL hot core. Source I has been considered

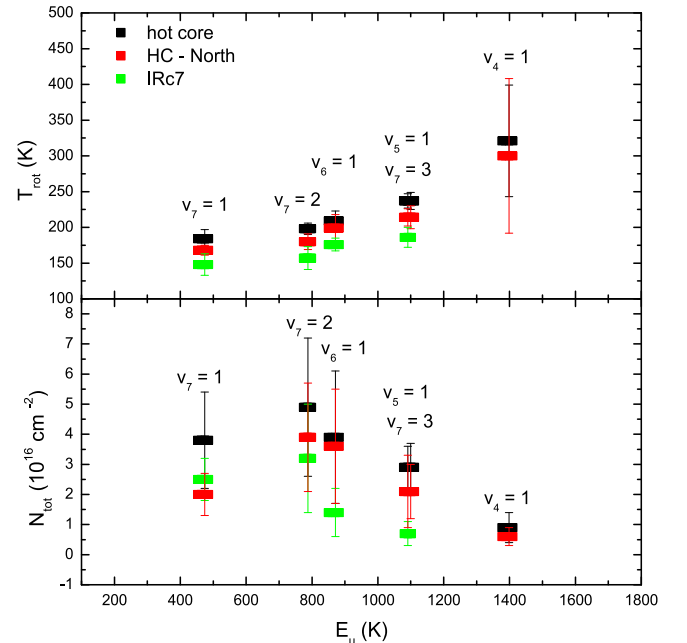


**Figure 8.** Plot of rotational temperature (top panel) and column density (bottom panel) as a function of upper-level energies ( $E_u$ ) toward three positions.

as the most likely external candidate based on the observations of lines and continuum (Blake et al. 1996; Wilson et al. 2000). However, there is offset between Source I and the peaks of vibrationally excited states of  $\text{HC}_3\text{N}$  (de Vicente et al. 2002).

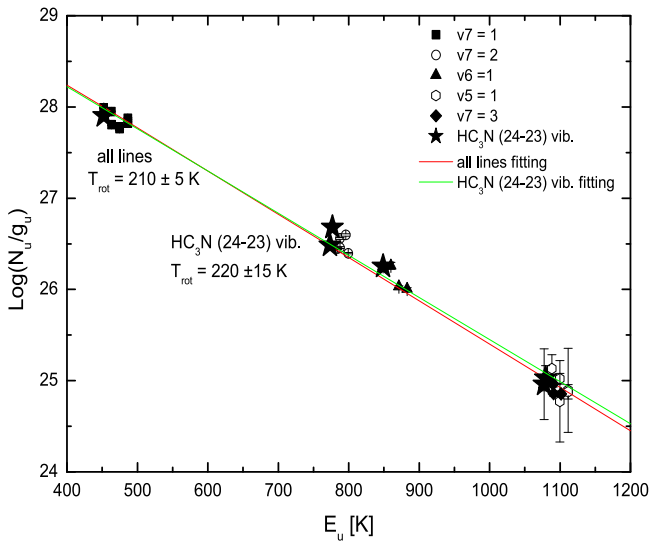


**Figure 9.** Rotational temperature diagram for observed HC<sub>3</sub>N lines. The red lines represent the fit of level population for  $v_7 = 1$  (squares),  $v_7 = 2$  (circles),  $v_7 = 3$  (diamond),  $v_6 = 1$  (triangles), and  $v_5 = 1$  (hexagons). The green lines fit the  $v_7 = 1$ ,  $v_7 = 2$ ,  $v_7 = 3$ ,  $v_6 = 1$ , and  $v_5 = 1$  with rotational  $J = 24$ – $23$  (marked with stars). All vibrationally excited HC<sub>3</sub>N lines have a rotational temperature of  $210 \pm 5$  K. As for the  $J = 24$ – $23$  of five vibrationally excited states, the resulting vibrational temperature is  $220 \pm 15$  K.

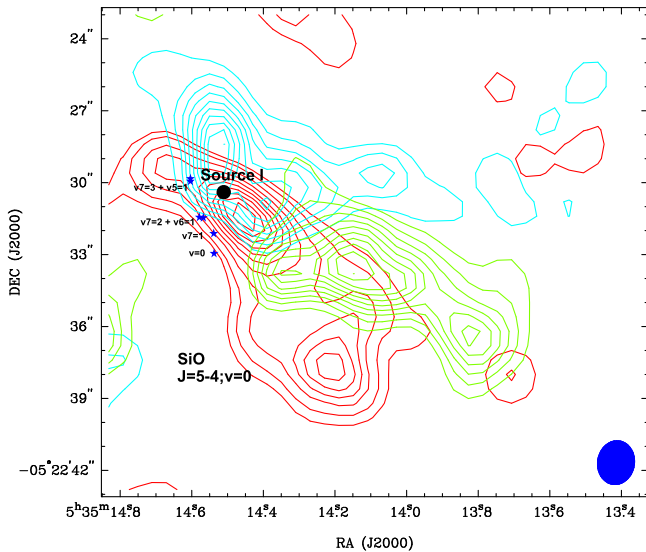


**Figure 10.** Overlays of the peak positions of HC<sub>3</sub>N in different vibrational states, and the integrated intensity contours of SiO ( $J = 5$ – $4$ ,  $v = 0$ ) emission (Zapata et al. 2012). The blue contours represent blueshifted gas with LSR velocities ranging from  $-15$  to  $-5$  km s<sup>-1</sup>. The red contours represent redshifted gas with LSR velocities ranging from  $+15$  to  $+22$  km s<sup>-1</sup>. The green contours represent redshifted high-velocity gas with LSR velocities ranging from  $+24$  to  $+30$  km s<sup>-1</sup>. The synthesized beam is shown in the bottom right corner. The blue, red, and green contours are 5%, 10%, 20%, 30%, 40%, 50%, 60%, 70%, 80%, 90%, and 100% of the emission peaks. The black solid circle indicates the radio Source I. The dark blue stars indicate the peak positions of HC<sub>3</sub>N  $v = 0$ , HC<sub>3</sub>N  $v_7 = 1$ , HC<sub>3</sub>N  $v_7 = 2$ , HC<sub>3</sub>N  $v_6 = 1$ , HC<sub>3</sub>N  $v_7 = 3$ , and HC<sub>3</sub>N  $v_5 = 1$ . The excitation gradient is along northeast–southwest orientation through emission peaks of HC<sub>3</sub>N vibrationally transitions as shown by dark blue stars.

Source I seems to not be a dominant source of excitation for HC<sub>3</sub>N. These observations throw doubt on radiation excitation of higher-energy HC<sub>3</sub>N transition. On the other hand, SiO is thought to be a shock tracer (Schilke et al. 1997). Outflows associated with Source I have been revealed by SiO ( $J = 5$ – $4$

and 8–7 transitions) with a northeast–southwest elongation (Zapata et al. 2012). In Figure 10, the peak positions of ground and vibrationally excited HC<sub>3</sub>N transitions in our observations were overlaid onto the SiO outflow (see also Figure 3 of Zapata et al. 2012). The excitation gradient of vibrationally excited HC<sub>3</sub>N lines show northeast–southwest orientation, which may indicate that higher-energy HC<sub>3</sub>N transitions are excited by interaction between pre-existing dense medium and shocks generated by SiO outflows, as suggested by other observations (Bally et al. 2011; Goddi et al. 2011; Zapata et al. 2011; Nissen et al. 2012; Peng et al. 2013).

## 5. Summary

Based on ALMA and IRAM 30 m observations of Orion KL, we have identified and imaged multiple vibrationally excited HC<sub>3</sub>N lines. The identified HC<sub>3</sub>N vibrationally excited transitions span a wide range of energy levels and allow us to perform a detailed LTE analysis to accurately derive physical parameters. The main conclusions are as follow:

1. Thirteen unblended lines of <sup>13</sup>C and <sup>15</sup>N isotopologues of HC<sub>3</sub>N in ground state, 41 unblended lines of HC<sub>3</sub>N in seven vibrational states ( $v_7 = 1$ ,  $v_7 = 2$ ,  $v_6 = 1$ ,  $v_7 = 3$ ,  $v_5 = 1$ ,  $v_4 = 1$  and  $v_4 = v_7 = 1$ ), and 23 unblended lines of three <sup>13</sup>C isotopologues (H<sup>13</sup>CCCN, HC<sup>13</sup>CCN and HCC<sup>13</sup>CN) in  $v_7 = 1$  and  $v_7 = 2$  are identified. The spectral profiles of vibrationally excited HC<sub>3</sub>N transitions extracted from ALMA and combined data are almost same.

2. The spatial distributions of these vibrational states are quite similar. Three main emission peaks (the hot core itself, IRc7, and HC-North) are identified. The morphologies of HC<sub>3</sub>N gas emissions with the ALMA data alone are similar to those by the combined data. The images of combined data are more extended than those by ALMA data alone, but the gas emissions of both ALMA and combined data peak at same positions.

3. Because the spectral profiles and peak intensity of vibrationally excited HC<sub>3</sub>N transitions are almost the same from both ALMA and combined data, one can safely use higher-energy transitions and isotopologues of HC<sub>3</sub>N from the ALMA data alone for data modeling. Rotational temperatures and column densities of the observed states range from 93 to 321 K and from  $1 \times 10^{14}$  to  $5 \times 10^{16}$  cm<sup>-2</sup>, 90 to 300 K and  $1 \times 10^{14}$  to  $4 \times 10^{16}$  cm<sup>-2</sup>, and 88 to 186 K and  $1 \times 10^{14}$  to  $3 \times 10^{16}$  cm<sup>-2</sup> for the hot core, HC-North, and IRc7, respectively. The hot core has the highest excitation temperature and column density, compared to HC-North and IRc7. Using the column density ratio of HC<sub>3</sub>N to its <sup>13</sup>C isotopologues in the  $v_7 = 1$  and  $v_7 = 2$  states, we derived an average <sup>12</sup>C/<sup>13</sup>C abundance ratio of  $52 \pm 24$  for Orion KL.

4. The emission peak of HC<sub>3</sub>N  $v = 0$  for the hot core is located southeast of Source I, whereas the emission peaks of HC<sub>3</sub>N in higher vibrational states (e.g.,  $v_7 = 3$  and  $v_5 = 1$ ) are located northeast of Source I. The line images also show that the emission peaks of vibrationally excited HC<sub>3</sub>N lines are moving from southeast to northeast with  $E_u$  increasing. Our LTE calculations suggested that higher-energy transitions have higher gas temperatures and lower column densities. Altogether, these results likely support the idea of the Orion KL hot core being externally heated. The emission peaks of vibrationally excited HC<sub>3</sub>N transitions in our observations are moving northeast along the major axis of the SiO outflow, which may indicate that higher-energy HC<sub>3</sub>N transitions are excited by

interaction between pre-existing dense medium and shocks generated by SiO outflows.

This paper makes use of the following ALMA data: ADS/JAO.ALMA#2011.0.00009.SV. ALMA is a partnership of ESO (representing its member states), NSF (USA), and NINS (Japan), together with NRC (Canada) and NSC and ASIAA (Taiwan), in cooperation with the Republic of Chile. The Joint ALMA Observatory is operated by ESO, AUI/NRAO, and NAOJ. This work has been supported by the National Natural Science Foundation of China under grant Nos. 11373026, 11373009, 11433004, 11433008, and the Joint Research Fund in Astronomy (U1331116 and U1631237) under cooperative agreement between the National Natural Science Foundation of China (NSFC) and Chinese Academy of Sciences (CAS), by the Top Talents Program of Yunnan Province (2015HA030), and by the Deutsche Forschungsgemeinschaft, DFG through project number SFB956.

## References

- Bally, J., Cunningham, N. J., Moeckel, N., et al. 2011, *ApJ*, 727, 113
- Belloche, A., Müller, H. S. P., Menten, K. M., et al. 2013, *A&A*, 559, 47
- Beuther, H., Zhang, Q., Greenhill, L. J., et al. 2005, *ApJ*, 632, 355
- Blake, G. A., Mundy, L. G., Carlstrom, J. E., et al. 1996, *ApJL*, 472, L49
- Blake, G. A., Sutton, E. C., Masson, C. R., & Phillips, T. G. 1987, *ApJ*, 315, 621
- Brouillet, N., Despois, D., Lu, X. H., et al. 2015, *A&A*, 576, A129
- Churchwell, E., Fell, M., Wood, D. O. S., & Massi, M. 1987, *ApJ*, 321, 516
- Clark, F. O., Brown, R. D., Godfrey, P. D., et al. 1976, *ApJL*, 210, L139
- Crockett, N. R., Bergin, E. A., Neill, J. L., et al. 2014, *ApJ*, 787, 112
- de Vicente, P., Martín-Pintado, J., Neri, R., & Rodríguez-Franco, A. 2002, *ApJL*, 574, L163
- Favre, C., Despois, D., Brouillet, N., et al. 2011, *A&A*, 532, A32
- Feng, S., Beuther, H., Henning, Th., et al. 2015, *A&A*, 581, 71
- Friedel, D. N., & Snyder, L. E. 2008, *ApJ*, 672, 962
- Garrod, R. T., Weaver, Widicus., Susanna, L., & Herbst, E. 2008, *ApJ*, 682, 283
- Gezari, D. Y., Backman, D. E., & Werner, M. W. 1998, *ApJ*, 509, 283
- Gezari, D. Y., Folz, W., Woods, L., & Varosi, F. 1992, *PASP*, 104, 191
- Goddi, C., Greenhill, L. J., Humphreys, E. M. L., Chandler, C. J., & Matthews, L. D. 2011, *ApJL*, 739, L13
- Goldsmith, P. F., Krotkov, R., & Snell, R. L. 1982, *ApJ*, 260, 147
- Goldsmith, P. F., Krotkov, R., & Snell, R. L. 1983, *ApJ*, 274, 184
- Goldsmith, P. F., Krotkov, R., & Snell, R. L. 1985, *ApJ*, 299, 405
- Goldsmith, P. F., & Langer, W. D. 1999, *ApJ*, 517, 209
- Gong, Y., Henkel, C., Thorwirth, S., et al. 2015, *A&A*, 581, 48
- Greenhill, L. J., Gezari, D. Y., Danchi, W. C., et al. 2004, *ApJL*, 605, L57
- Kaufman, M. J., Hollenbach, D. J., & Tielens, A. G. G. M. 1998, *ApJ*, 497, 276
- Langer, W. D., & Penzias, A. A. 1990, *ApJ*, 357, 477
- Langer, W. D., & Penzias, A. A. 1993, *ApJ*, 408, 539
- Liu, S., Girart, J. M., Remijan, A., & Snyder, L. E. 2002, *ApJ*, 576, 255
- Masson, C. R., & Mundy, L. G. 1988, *ApJ*, 324, 538
- Menten, K. M., & Reid, M. J. 1995, *ApJ*, 445, 157
- Menten, K. M., Reid, M. J., Forbrich, J., & Brunthaler, A. 2007, *A&A*, 474, 515
- Möller, T., Bernst, I., Panoglou, D., et al. 2013, *A&A*, 549, 21
- Möller, T., Endres, C., & Schilke, P. 2015, arXiv:150804114M
- Müller, H. S. P., Schlöder, F., Stutzki, J., & Winnewisser, G. 2005, *JMoSt*, 742, 215
- Müller, H. S. P., Thorwirth, S., Roth, D. A., & Winnewisser, G. 2001, *A&A*, 370, 49
- Neill, J. L., Crockett, N. R., Bergin, E. A., et al. 2013, *ApJ*, 777, 85
- Nissen, H. D., Cunningham, N. J., Gustafsson, M., et al. 2012, *A&A*, 540, A119
- Okumura, S.-i., Yamashita, T., Sako, S., et al. 2011, *PASJ*, 63, 8230
- Palau, A., Fuente, A., Girart, J. M., et al. 2011, *ApJL*, 743, L32
- Peng, T.-C., Despois, D., Brouillet, N., et al. 2013, *A&A*, 554, A78
- Persson, C. M., Olofsson, A. O. H., Koning, N., et al. 2007, *A&A*, 476, 807
- Pickett, H. M., Poynter, R. L., Cohen, E. A., et al. 1998, *JQSRT*, 60, 883
- Remijan, A., Snyder, L. E., Friedel, D. N., et al. 2003, *ApJ*, 590, 314
- Sánchez-Monge, Á., Beltrán, M. T., Cesaroni, R., et al. 2014, *A&A*, 569, A11
- Sánchez-Monge, Á., Cesaroni, R., Beltrán, M. T., et al. 2013, *A&A*, 552, L10
- Sault, R. J., Teuben, P. J., & Wright, M. C. H. 1995, in ASP Conf. Series, Vol. 77, *Astronomical Data Analysis Software and Systems IV*, ed. R. A. Shaw, H. E. Payne, & J. J. E. Hayes (San Francisco, CA: ASP), 433
- Savage, C., Apponi, A. J., Ziurys, L. M., & Wyckoff, S. 2002, *ApJ*, 578, 211
- Schilke, P., Benford, D. J., Hunter, T. R., Lis, D. C., & Phillips, T. G. 2001, *ApJS*, 132, 281
- Schilke, P., Groesbeck, T. D., Blake, G. A., & Phillips, T. G. 1997, *ApJS*, 108, 301
- Shuping, R., Morris, M., & Bally, J. 2004, *AJ*, 128, 363
- Simpson, J. P., Colgan, S. W. J., Erickson, E. F., et al. 2006, *ApJ*, 642, 339
- Snyder, L. E., Lovas, F. J., Hollis, J. M., et al. 2005, *ApJ*, 619, 914
- Tercero, B., Cernicharo, J., Pardo, J. R., & Goicoechea, J. R. 2010, *A&A*, 517, A96
- Thorwirth, S., Müller, M., & Winnewisser, H. S. P. 2000, *JMoSp*, 204, 133
- Wang, K. S., Kuan, Y. J., Liu, S. Y., & Charnley, S. B. 2010, *ApJ*, 713, 1192
- Widicus Weaver, S. L., & Friedel, D. N. 2012, *ApJS*, 201, 16
- Wilson, T. L., Gaume, R. A., Gensheimer, P., & Johnston, K. J. 2000, *ApJ*, 538, 665
- Wright, M. C. H., Plambeck, R. L., & Wilner, D. J. 1996, *ApJ*, 469, 216
- Wu, Y. F., Liu, T., & Qin, S. L. 2014, *ApJ*, 791, 123
- Wynn-Williams, C. G., Genzel, R., Becklin, E. E., & Domnes, D. 1984, *ApJ*, 281, 172
- Wyrowski, F., Schilke, P., & Walmsley, C. M. 1999, *A&A*, 341, 882
- Zapata, L. A., Rodríguez, L. S., Schmid-Burgk, J., et al. 2012, *ApJL*, 754, 17
- Zapata, L. A., Schid-Burgk, J., & Menten, K. M. 2011, *A&A*, 529, A24